| 1  | Measurement report: Observational insights into the impact of dust  |
|----|---|
| 2  | transport on atmospheric dicarboxylic acids in ground region and free   |
| 3  | troposphere   |
| 4  | Minxia Shen <sup>1</sup> , Weining Qi <sup>1</sup> , Yali Liu <sup>1,2</sup> , Yifan Zhang <sup>1,2</sup> , Wenting Dai <sup>1,3</sup> , Lu Li <sup>1</sup> , Xiao Guo <sup>1</sup> , |
| 5  | Yue Cao <sup>1,2</sup> , Yingkun Jiang <sup>1,2</sup> , Qian Wang <sup>1</sup> , Shicong Li <sup>1</sup> , Qiyuan Wang <sup>1,3</sup> , Jianjun Li <sup>1,3*</sup>                    |
| 6  |   |
| 7  | <sup>1</sup> State Key Laboratory of Loess Science, Institute of Earth Environment, Chinese   |
| 8  | Academy of Sciences, Xi'an 710061, China  |
| 9  | <sup>2</sup> Xi'an Institute for Innovative Earth Environment Research, Xi'an, China  |
| 10 | <sup>3</sup> National Observation and Research Station of Regional Ecological Environment Change  |
| 11 | and Comprehensive Management in the Guanzhong Plain, Xi'an, China   |
| 12 |   |
| 13 |   |
| 14 | *Corresponding author: Jianjun Li, e-mail address: lijj@ieecas.cn   |
| 15 |   |

Abstract. This study investigated the vertical distribution of PM<sub>2.5</sub> and size-segregated aerosols at the foot and top of Mount Hua in Northwest China, focusing on C2 formation and its  $\delta^{13}C$  characteristics influenced by dust transport. Under non-dust conditions, PM<sub>2.5</sub> and diacids concentrations at the foot were 4.5 and 2.1 times higher than those at the top, with stronger local anthropogenic signals (C<sub>9</sub>, 5.67 times higher) and pronounced diurnal day-night differences for diacids variation. Higher C<sub>2</sub>/C<sub>4</sub> (5.84 vs. 4.74), C<sub>3</sub>/C<sub>4</sub> (1.04 vs. 0.56) ratios and δ<sup>13</sup>C values (-21.5‰ vs. -27.6‰) at the top indicated photochemical aging during aerosol transport. C<sub>2</sub> concentration was positively correlated with aerosol liquid water content and its size distribution pattern matched with precursors, confirming aqueous-phase oxidation as the dominant formation pathway. During dust events, PM<sub>2.5</sub> concentrations at the foot and top reached 457 μg m<sup>-3</sup> and 165 μg m<sup>-3</sup>, but C<sub>2</sub> concentrations in PM<sub>2.5</sub> decreased by 59% (foot) and 25% (top), while  $\delta^{13}$ C values of C<sub>2</sub> exhibited a significant positive shift (foot: -27.6% to -23.9%; top: -21.5% to -13.2%), attributed to alkaline dust catalyzing <sup>13</sup>C-enriched oxalate formation. mGly became the second most abundant acid due to enrichment on dust-particle surfaces. Size-segregated data revealed decreased fine-particle C2 but increased coarse-particle C<sub>2</sub>, elevating the coarse-to-fine particle ratio from 0.3~0.4 to 0.6~1.1. These findings offer valuable insights into the altitude-dependent transformation of SOA affected by dust transport, enhancing our understanding of mountain atmospheric chemistry and regional air quality.

- **Keywords**: Dicarboxylic acids, dust particles, size distribution, stable carbon isotopes (δ<sup>13</sup>C),
- 35 aqueous-phase oxidation, heterogeneous reactions

16

17

18

19

20

2122

23

24

25

26

27

28

29

30

31

32

#### 1 Introduction

36

37 Dust cycling is crucial to Earth's climate system (Maher et al., 2010; Liang et al., 2022). Mineral particles from dust storms absorb and scatter solar radiation (Kumar et al., 2014), 38 altering regional heat balance and cloud properties, which in turn affects precipitation 39 (Mahowald et al., 2014; Kok et al., 2023; Marx et al., 2024; Xu-Yang et al., 2025). They 40 41 also act as effective ice-nucleating particles (INPs) in mixed-phase clouds, regulating ice 42 formation and the radiation budget (Fan et al., 2016; Vergara-Temprado et al., 2018; Kawai, et al., 2021; Chen et al., 2024). Dust particles often contain high levels of salts, bacteria, and 43 heavy metals, posing potential risks to human health and plant growth (Yamaguchi et al., 2016; 44 Luo et al., 2024). Dust not only degrades impairs air quality locally but also undergoes long-45 range near its source and can be transported, over long distances by winds, ultimately 46 47 impacting affecting both the climate on hemispheric and global climate scales ystems (Pan et al., 2025). During transport, mineral dust may undergo heterogeneous reactions, forming 48 49 secondary <u>aerosols</u> substances that aid cloud formation (Wang et al., 2020; Bikkina et al., 2023). The large surface area of these particles facilitates reactions that alter radiation transfer and 50 51 photolysis rates (Sullivan et al., 2007a). 52 Over the past 500 years, East Asia has been frequently hit by dust storms (Zhang et 53 al., 2021; Wu et al., 2022). The Taklimakan and Gobi Deserts, the primary sources of East Asian dust, emit over 800 million tons of dust to downwind areas annually (Sullivan et al., 54 2007b; Wang et al., 2015; Ren et al., 2019; Zhu and Liu, 2024). Northwestern and northern 55 56 China, frequently experience dusty weather due to these desert emissions (Gui et al., 2022; Liang et al., 2022). In spring 2023, Mongolia contributed over 42% of the dust 57 58 concentration in northern China (Chen et al., 2023). Although dust storms are more common in China during spring (Sun et al., 2001), a large-scale, high-intensity dust storm 59 60 hit northern China on January 10, 2021. This severe dust storm, Ooriginating from in southern Mongolia and - China's western Inner Mongolia, triggered - it was intense and 61 62 far reaching, causing rapid air quality deterioration across downwind regions in the affected areas (Figure S1). Our synchronized field observations of PM<sub>2.5</sub> and size-segregated aerosols 63

at the top of Mount Hua and on the ground in the winter of 2021 successfully captured this large-scale dust event, as shown in Fig. S1, extensively covering Northern China and the Guanzhong Plain. Liu et al. (2024) compared and analyzed the concentrations and size distributions of water-soluble inorganic ions during dust and non-dust periods, findingResults show that the impact of dust storms have a less pronounced impact on ground aerosols in the Guanzhong Plain is weaker than on that in the free troposphere of the Guanzhong Plain (Liu et al., 2024),. Nevertheless, the specific mechanisms through which dust affects organic components, particularly secondary organic aerosol (SOA) and their precursors but the specific effects of dust on organic matter in the ground and troposphere remain unclear and require further study. To investigate these processes, this study focuses on dicarboxylic acids (diacids), which serve as key tracers for SOA (Xu et al., 2022). As important components of water-soluble organic carbon, diacids are widely distributed in the atmosphere from the surface layer to the free troposphere (Fu et al., 2008; Myriokefalitakis et al., 2011). Conventional theory suggests that aqueous-phase chemical reactions occur predominantly in submicron particles containing water or cloud droplets (Lim et al., 2010; Ervens et al., 2011; Lamkaddam et al., 2021). However, field observations have reported the coexistence of oxalate and nitrate in supermicron particles during dust events (Falkovich and Schkolnik, 2004; Sullivan et al., 2007a; Wang et al., 2015; Xu et al., 2020). To explain this, Wang et al. (2015) proposed that the reaction of nitric acid and/or nitrogen oxides with dust generates (Ca(NO<sub>3</sub>)<sub>2</sub>), which absorbs water vapor to form an aqueous phase on the dust surface. This enables the partitioning of gas-phase watersoluble organic precursors into this aqueous phase, followed by their further oxidation to form oxalic acid (C2). Research by Li et al. (2025) provides direct evidence for this mechanism, showing that aqueous nitrate coatings (Ca(NO<sub>3</sub>)<sub>2</sub>), due to their very low deliquescence relative humidity (absorbing water at atmospheric RH > 8%), effectively promote the formation of aqueous secondary organic aerosols (aqSOA). Thus, aged dust surfaces provide critical reactive interfaces for aqSOA formation.

64

65

66

67

68

69

70

71

72

73

74

75

76

77

78

79

80

81

82

83

84

85

86

87

88

89

New research shows that nitrate aged dust plays a crucial role in secondary organic aerosol (SOA) formation through aqueous phase reactions (Li et al., 2025). As important SOA constituents, dicarboxylic acids (diacids) are ubiquitously distributed from the surface layer to the free troposphere. Due to their low gas phase reactivity, these compounds are primarily removed via dry deposition, wet deposition, and other heterogeneous processes. Their photochemical reactivity on mineral dust surfaces exhibits distinct carbon chain length dependence, significantly influencing atmospheric organic transformations and aerosol properties (Ponezek et al., 2019). In Asian dust systems, diacids form insoluble complexes with divalent cations (e.g., Ca<sup>2+</sup>) and undergo photocatalytic reactions with transition metals (e.g., Fe<sup>2+</sup>/Fe<sup>3+</sup>), generating radical oxidants that promote oxalate oxidation and iron reduction (Deguillaume et al. 2005).

Oxalic acid (C<sub>2</sub>), a major atmospheric diacid, has a global tropospheric burden of 0.2–0.3 Tg and comprises 5–9% of atmospheric water soluble organic carbon (Myriokefalitakis et al., 2011). Alkaline mineral particles, like Asian dust, adsorb acidic C<sub>2</sub> readily, while acidic carbonaceous particles are resistant to further adsorption (Yu et al., 2019). The daily variation

Tg and comprises 5–9% of atmospheric water soluble organic carbon (Myriokefalitakis et al., 2011). Alkaline mineral particles, like Asian dust, adsorb acidic C<sub>2</sub>-readily, while acidic carbonaceous particles are resistant to further adsorption (Yu et al., 2019). The daily variation of C<sub>2</sub> in East Asian mineral dust outflow indicates that its mixture originates from the photochemical transformation of volatile organic compounds (VOCs) (Sullivan et al., 2007b). Mochida et al. (2003) investigated the size distribution of C<sub>2</sub>, malonic acid (C<sub>3</sub>) and succinic acid (C<sub>4</sub>) in aerosols from the Western Pacific and East Asian coasts. They discussed the adsorption of gas-phase diacids on sea salt particles and the possible formation of solid oxalates, which may enhance the absorption of gaseous C<sub>2</sub>-by aerosol particles.

Tropospheric aerosols in high mountain areas are significantly influenced by long-range transport of surface pollutants, making them more representative of regional atmospheric quality. Our previous study (Shen et al., 2023), we investigated the vertical distribution of diacids and the formation mechanisms of C<sub>2</sub> in PM<sub>2.5</sub> at different elevations of Mount Hua during the summer. The results demonstrated that summer daytime valley winds on Mount Hua can transport organic acids emitted from the foot to the top, significantly thereby altering the chemical composition of the free troposphere and establishing distinct formation pathways of

C<sub>2</sub> at different altitudes. while distinct C<sub>2</sub> formation pathways were observed between the top and foot sites. This study examines aerosol vertical distribution characteristics in winter. Low temperatures cause a significant reduction in the boundary layer height over Mount Hua, which inhibits the diffusion of local pollutants to the top. Consequently, the top remains in a free tropospheric environment where aerosols originate primarily from long-range transport from dust source regions (Liu et al., 2024). During the observational period, we documented a major dust event in which particles from dust source regions were directly transported to the top. There, they mixed with local anthropogenic pollutants, triggering complex atmospheric chemical reactions that resulted in notable vertical differences in aerosol chemical properties. However, the influence of heterogeneous reactions on dust aerosol surfaces on the generation of organic acids, particularly their role in modifying C<sub>2</sub> formation mechanisms at different altitudes remains unclear. Therefore, using Here, we further analyzed the observational data from a typical dust event their winter -of-20201, during which a typical dust event occurred. Tthis study focuses on examining aims to explore the impacts of winter-dust transport events on the molecular distribution, particle size characteristics of diacids, and the formation mechanisms of C2. Our findings will provide new insights The work aims to elucidate the key into the important role of heterogeneous chemical reactions on the surfaces of dust aerosols in the formation of secondary organic aerosolsSOA, providing new insights into regional atmospheric chemical processes during dust events.

### 2 Experimental and methods

## 2.1 Sample collection

119

120

121

122

123

124

125

126

127

128

129

130

131

132

133

134

135

136

137

138

139

140

141

142

143

144

145

146

Samples were collected simultaneously at the free troposphere and the ground surface during December 17, 2020 to January 12, 2021. The sampling site at the ground surface is located on Yinquan Road, Huayin City, Weinan (34°31'N, 110°04'E; ~500 m a.s.l) (referred to as "Foot"), while alpine sampling site is located at the summit of the west peak of Mount Hua (34°28'N, 110°05'E; ~2065 m a.s.l) (referred to as "Top") (Fig. 1). PM<sub>2.5</sub> aerosol samples was collected using medium-flow sampler (HC-1010, China Qingdao Company, China) at a flow rate of 100 L min<sup>-1</sup> with a duration of 11 hours for each sample during the day (from 08:00 to

19:00) and night (from 20:00 to 07:00 the next day). A total of 54 samples were collected at both the alpine region and ground. The size-segregated samples were collected for ~71 h in each set using an Andersen multi-stage impactor (Andersen, Thermo electronic, USA) at a flow rate of 28.3 L min<sup>-1</sup> with 9 size bins as < 0.4, 0.4–0.7, 0.7–1.1, 1.1–2.1, 2.1–3.3, 3.3–4.7, 4.7–5.8, 5.8–9.0 and > 9.0  $\mu$ m, respectively. In a total of 9 sets of size-segregated samples were collected. All the samples were collected onto pre-combusted (450°C for 6 h) quartz fiber filters produced by Whatman, UK. After sampling, the filters were stored in -18°C until analysis.

The concentrations of organic carbon (OC) and elemental carbon (EC) in PM<sub>2.5</sub> samples

### 2.2 Laboratory Analysis

147

148

149

150

151

152

153

154

155

156

157

158

159

160

161

162

163

164

165

166

167

168

169

170

171

172

173

respectively.

## 2.2.1 Determination of carbonaceous species and water-soluble inorganic ions

were determined quantified using a DRI Model 2001 carbon analyzer (Atmoslytic Inc., USA), following the IMPROVE thermal/optical reflectance (TOR) protocol (Cao et al., 2007). A 0.526 cm<sup>2</sup> filter punch was heated stepwise in pure helium (at 120 °C, 250 °C, 450 °C, and 550 °C) followed by heating in a 2% oxygen/helium atmosphere (at 550 °C, 700 °C, 800 °C). The method detection limits were 0.41  $\mu g$  cm<sup>-2</sup> for OC and 0.03  $\mu g$  cm<sup>-2</sup> for EC. Water-soluble components were extracted from a quarter of each filter using 40 mL of ultrapure water (Milli-Q, 18.2 MΩ, Merck, France) via a combined process of 1-hour ultrasonication and 1-hour mechanical shaking. After filtration through a 0.45 µm membrane, the extracts were preserved at 4 °C for subsequent analysis. Water-soluble inorganic ions (NH<sub>4</sub><sup>+</sup>, K<sup>+</sup>, Mg<sup>2+</sup>, Ca<sup>2+</sup>, Cl<sup>-</sup>, NO<sub>3</sub><sup>-</sup>, and SO<sub>4</sub><sup>2-</sup>) were analyzed by ion chromatography (Metrohm 940, Switzerland). Anions and cations were separated using an IonPac AS23 column and an IonPac CS12A column, with 9.0 mM Na<sub>2</sub>CO<sub>3</sub> and 20 mM methanesulfonic acid as eluents, respectively (Zhang et al., 2011). Concurrently, water-soluble organic carbon (WSOC) was determined using a total organic carbon (TOC) analyzer (TOC-L CPH, Shimadzu, Japan) (Li et al., 2019). The detection limits for inorganic ions ranged from 0.008 to 0.022 µg m<sup>-3</sup>, while those for total carbon (TC) and inorganic carbon (IC) were 0.07 mg L<sup>-1</sup> and 0.08 mg L<sup>-1</sup>,

Aerosol liquid water content (ALWC) was <u>calculated using the ISORROPIA-II model</u> (Fountoukis and Nenes, 2007), based on the concentrations of water-soluble inorganic ions (SO<sub>4</sub><sup>2=</sup>, NH<sub>4</sub><sup>±</sup>, CI<sup>-</sup>, NO<sub>3</sub><sup>=</sup>, Ca<sup>2±</sup>, K<sup>±</sup>, and Mg<sup>2±</sup>) and meteorological <u>parameters including fields</u> (i.e., relative humidity (RH) and temperature (T). ) in the ISORROPIA-II model developed by Fountoukis and Nenes (2007). Meteorological data for the top and the foot were obtained from the Mount Hua Meteorological Station and the Huayin Meteorological Bureau, respectively. All statistical analyses were performed using SPSS.

## 2.2.2 Determination of dicarboxylic acids and related compounds

174

175

176

177

178

179

180

181

182

183

184

185

186

187

188

189

190

191

192

193

194

195

196

197

198

199

200

201

The analysis of diacids, keto-carboxylic acids, and α-dicarbonyls in analysis, PM<sub>2.5</sub> and size-segregated aerosols samples, werewas conducted based on an established derivatization method (Shen et al., 2022). A quarter of each filter was extracted by ultrasonicating one-quarter of each filter in ultrapure water (Milli-Q, 18.2 M $\Omega$ , Merck, France) for three sequential 15minute intervals. To maximize the recovery of low-molecular-weight acids (e.g., C<sub>2</sub>), the extracts were alkalized were adjusted to pH 8.5-9.0 using with 0.1 M KOH prior to the concentration stepbefore drying. The aqueous extracts were concentrated to near-dryness under vacuum in a water bath maintained at 55 °C (evaporation was halted immediately after the disappearance of the last drop of solvent). The Dried dried residues were derivatized underwent derivatization with 14% BF<sub>3</sub>/n-butanol at 100°C for 1 hour to convert transform carboxyl groups into dibutyl esters and oxo groups into dibutoxyacetals. After the reaction, the derivatives were sequentially dissolved in n-hexane, acetonitrile, and pure water, followed by triple extraction via vortex mixing to remove water-soluble inorganic substances. The aqueous lower layer was removed using a Pasteur pipette. Organic derivatives were purified via triple water-washing of the The n-hexane layer was concentrated by rotary evaporation and N<sub>2</sub> blowdown, and reconstituted in 100 µL n-hexane, and finally analyzed for by GC-FID analysis (HP 6890, Agilent Technologies, USA) (Wang et al., 2012). The recovery of the target compounds was 83% for C<sub>2</sub> and ranged from 87% to 110% for other diacids.

Stable carbon isotopic compositions ( $\delta^{13}$ C) of <u>oxalic acidC</u><sub>2</sub> were determined using gas chromatography–isotope ratio mass spectrometry (GC-IRMS; Delta V Advantage, Thermo

Fisher Scientific, Franklin, MA, USA) following established protocols (Kawamura and Watanabe, 2004). To ensure analytical precision (standard deviation < 0.2‰), derivatized samples were analyzed in triplicate. Final  $\delta^{13}$ C values of free oxalic acid were calculated via mass-balance correction to account for isotopic contributions from the BF<sub>3</sub>/n-butanol derivatizing agent.

### 3 Results and discussion

# 3.1 Vertical differences in PM<sub>2.5</sub> chemical composition at the foot and top of Mount Hua during non-dust periods

During winter—non-dust periods, significant vertical differences were observed in the chemical composition of PM2.5 ehemical composition between the foot and top of Mount Hua. The average PM2.5 concentration at the foot was(127  $\pm$  48  $\mu g$  m $^{-3}$ ) was 4.5 times higher than that at the top (28  $\pm$  14  $\mu g$  m $^{-3}$ ), with a mean difference of 99  $\mu g$  m $^{-3}$  (95% CI: 86 to 113; t (61.05) = 14.60, p < 0.001) (Supplementary Table S1 and Table S3a), approximately 4.5 times higher than the top concentration of 28  $\pm$  14  $\mu g$  m $^{-3}$  (Supplementary Table S1).

This vertical gradient was apparent not only in PM2.5 mass concentrations but also in their chemical composition, as carbonaceous Carbonaceous aerosols components and water-soluble ions were significantly enriched accumulated in significantly higher amounts at the foot (all p  $\leq$  0.001; Table S3a). Diacids and their derivatives, which are As key components constituents of water-soluble organic carbon (WSOC) (Kawamura et al., 2016; Yang et al., 2020), showed particularly strong spatial variation. the total concentrations of diacids at the foot (1808  $\pm$  1280 ng m $^{-3}$ ) were was approximately 2.1 times higher than those at the top (860  $\pm$  534 ng m $^{-3}$ ), with a mean difference of 718 ng m $^{-3}$  (95% CI: 453 to 983; t (69.15) = 5.40, p < 0.001; Table S3b).

The spatial difference was most pronounced for azelaic acid (C<sub>9</sub>), a biomarker of biomass

burning (Kalogridis et al., 2018; Shen et al., 2022) showed the difference, with the

concentration at the foot being (153  $\pm$  110 ng m<sup>-3</sup>) being 5.7 times higher than that and at the

top ( $27 \pm 18 \text{ ng m}^{-3}$ ), corresponding to a mean difference of 126 ng m<sup>-3</sup> (95% CI: 95 to 156; t

(54.77) = 8.24, p < 0.001; Table S3b). , indicating a 5.7-fold higher concentration at the foot.

Consequently, Tthe contribution ratios of C<sub>9</sub> to total diacids awas substantially greater at the foot (at the two sites were 8.5%) than at the topand (3.2%) (Fig. 2b), respectively.

229

230

231

232

233

234

235

236

237

238

239

240

241

242

243

244

245

246

247

248

249

250

251

252

253

254

255

256

Correlation analysis of PM<sub>2.5</sub> and its chemical components revealed no significant relationship between the two sites during winter, contrasting with the positive correlations observed in summer (Shen et al., 2023). Combined with ion compositiondata and backtrajectory analysis from Liu et al. (2024), these findings indicate that pollutants at the top primarily originated from regional transport in-from the northwestern direction with minimal vertical mixing, while the components at the foot of the mountain were mainly controlled by local emission sources. This conclusion was further supported by diurnal variation patterns.

Day-night differences provide further evidence supporting this conclusion. At the foot of the mountain, PM<sub>2.5</sub>, ionic components, and carbonaceous components (except for NO<sub>3</sub><sup>-</sup> and NH<sub>4</sub><sup>+</sup>) all showed significant day-night differences (p < 0.05; Table S4a). Among the diacids, methylglyoxal (mGly) exhibited the most pronounced significant day-night differences, with methylglyoxal (mGly) showing the most pronounced variation (daytime: 128 ± 49 ng m<sup>-3</sup>, 47% higher than nighttime:  $87 \pm 42$  ng m<sup>-3</sup>, p < 0.001; Fig. S2, Table S4b). As the terminal product of diacids photo-oxidation (Kawamura and Sakaguchi, 1999) Oxalic acid (C2), as the terminal product of diacids (Kawamura and Sakaguchi, 1999), C<sub>2</sub> also displayed marked day-night differences diurnal variation (daytime:  $766 \pm 552$  ng m<sup>-3</sup> vs. nighttime:  $585 \pm 497$  ng m<sup>-3</sup>, p = 0.023), reflecting strong anthropogenic influence on ground-level photochemistry. In contrast,  $\underline{C}_2$  at the top of the Mount Hua (daytime:  $312 \pm 224$  ng m<sup>-3</sup> vs. nighttime:  $299 \pm 186$  ng m<sup>-3</sup>; p = 0.941) and its precursors -concentrations showed no significant clear day-night differences diurnal fluctuation (p = 0.341-0.917; Table S4c), consistent with the patterns of PM<sub>2.5</sub> (p = 0.979), OC (p = 0.766), and other major components (Table S4a). -indicating that the highaltitude environment is primarily dominated by regional transport with relatively limited local photochemical contributions. Such stability is a typical characteristic of high-altitude sites located above the planetary boundary layer, primarily governed by regional transport processes (Fu et al., 2008; Li et al., 2012; Meng et al., 2014), indicating that aerosol processes in the free troposphere differ from those at ground level. In this high-altitude environment, in-cloud

processes represent a key pathway for aqSOA formation. Studies have shown that C<sub>2</sub> mainly originates from the in-cloud oxidation of precursors such as glyoxal (Gly) and isoprene (Warneck, 2003; Lim et al., 2005; Carlton et al., 2006), a mechanism supported by global model simulations (Myriokefalitakis et al., 2011). Additionally, the photochemical decomposition of C<sub>2</sub> following its association with Fe-containing particles in clouds (Zhang et al., 2019) also contributes to the stable distribution of organic acid concentrations at high altitudes.

Aerosol aging indicators further confirmed distinct oxidation processes between different altitudes. According to existing research, succinic acid ( $C_4$ ) can be via hydroxylation to generate  $C_2$  and malonic acid ( $C_3$ ), while  $C_3$  can be further converted to  $C_2$  through intermediates such as hydroxymalonic acid or ketomalonic acid (Kawamura et al. 1993; Kunwar and Kawamura, 2014; Hoque et al., 2017). Therefore, the  $C_2/C_4$  and  $C_3/C_4$  ratios are widely used as effective indicators for assessing the extent of photochemical aging in organic aerosols (Kawamura et al., 2016; Meng et al., 2018; Shen et al., 2022). In this study, the top of Mount Hua, the  $C_2/C_4$  ratio at the top of Mount Hua reached was  $5.84 \pm 0.32$ , while and the  $C_3/C_4$  ratio was  $1.04 \pm 0.08$ , both significantly higher than the corresponding values at the foot  $(4.74 \pm 0.28)$  and  $0.56 \pm 0.05$ , respectively; Fig. 2c). These results are consistent with reports from high-altitude areas such as Mount Tai (Wang et al., 2009; Meng et al., 2018) and Mount Hua (Meng et al., 2014), collectively confirming that the atmosphere undergoes more significant photochemical aging during long-range transport at high altitudes. —elevated molecular ratios clearly indicate more advanced photochemical aging processes occurring during high altitude atmospheric transport (Meng et al., 2018).

This study compared the correlations between C<sub>2</sub> and its key precursors at the foot and top of Mount Hua (Fig. 3a–d, 3i–l), revealing differences in atmospheric oxidation pathways across altitudes. Building on this, the synergistic effects of inorganic ions and ALWC on C<sub>2</sub> formation were investigated (Fig. 3e–h, 3m–p), thereby elucidating the aqueous-phase reaction mechanisms and the role of environmental factors such as humidity in C<sub>2</sub> generation. Results showed that were observed between C<sub>2</sub> exhibited the strongest correlation with C<sub>2</sub> and its major

precursors at both sites, with glycolic acid ( $\omega C_2$ ) exhibiting the strongest relationship ( $R^2$  = 285 0.88 at the foot,  $R^2 = 0.95$  at the top, p < 0.01; Fig. 3 d, 1). Other key precursors included Gly 286  $(R^2 = 0.57 - 0.67, p < 0.01; Fig. 3b, 3j), mGly (R^2 = 0.58 - 0.85, p < 0.01; Fig. 3a, 3i), and pyruvic$ 287 acid (Pyr:  $R^2 = 0.80 - 0.81$ , p < 0.01; Fig. 3c, 3k). These correlation characteristics confirm that 288 aqueous-phase oxidation serves as the primary formation pathway for C2 under non-dust 289 conditions (Deshmukh et al., 2017; Du et al., 2022). The consistently higher correlation 290 coefficients at the top further substantiate the enhancing effect of prolonged atmospheric 291 292 processes on secondary organic aerosol formation. Contrary to previous studies (Meng et al., 2018; Wang et al., 2012; Meng et al., 2018), we 293 found that  $C_2$  correlated more strongly with  $NO_3^-$  ( $R^2 = 0.79$ , p < 0.01; Fig. 3f) than with  $SO_4^{2-}$ 294  $(R^2 = 0.71, p < 0.01; Fig. 3e)$  at the foot, reflecting the promoting effect of local anthropogenic 295 emissions on nitrate formation. The difference mainly stems from strong influences of local 296 anthropogenic emissions (e.g., traffic and industrial activities) at the foot, which provide 297 abundant NO<sub>x</sub> and lead to an increased proportion of NO<sub>3</sub><sup>-</sup> in PM<sub>2.5</sub>. Since NO<sub>3</sub><sup>-</sup> is more 298 hygroscopic than SO<sub>4</sub><sup>2-</sup>, its elevated concentration further enhances ALWC, thereby promoting 299 aqSOA formation and intensifying heterogeneous reaction processes (Huang et al., 2025). In 300 contrast, at the top of Mount Hua, C<sub>2</sub> exhibited a higher showed stronger correlation with SO<sub>4</sub><sup>2-</sup> 301  $(R^2 = 0.63, p < 0.01; Fig. 3m)$  than with  $NO_3^-$  ( $R^2 = 0.37, p < 0.01; Fig. 3n$ ). This phenomenon 302 303

is closely related to the active in-cloud processes in the free troposphere mentioned above.

SO<sub>4</sub><sup>2-</sup> at the top primarily originates from the oxidation of SO<sub>2</sub> within cloud droplets

(Yermakov et al., 2023), a process dominated by heterogeneous reactions (Wang et al., 2025).

Meanwhile, cloud droplets also provide key reaction media for the aqueous-phase

photooxidation of  $C_2$  precursors such as Gly and  $\omega C_2$  (Warneck, 2003).

304

305

306

307

308

309

310

311

312

Aerosol Liquid water content (ALWC) exhibited a humidity-dependent threshold effect on C<sub>2</sub> formation the oxidation process. Under RH<75% During the sampling period, ALWC was positively correlated with  $C_2$  concentration ( $R^2 = 0.36\text{-}0.44$ , p < 0.01; Fig. 3g, 3o), reflecting the promotion of precursor dissolution and oxidation by the expansion of the aqueous phase. However, when relative humidity (RH) exceeded 75%, supersaturation shifted the gasparticle partitioning equilibrium, causing  $C_2$  concentrations to decrease with increasing ALWC. After excluding high-humidity data, the correlation between ALWC and  $C_2$  significantly strengthened ( $R^2 = 0.59$ , p < 0.01; Fig. 3h, 3p), confirming that aqueous-phase oxidation is the primary pathway for  $C_2$  formation during non-dust periods. This finding complements the research by Yang et al. (2022) on the synergistic effects of humidity and pH, jointly revealing the complex regulatory mechanisms of  $C_2$  formation under different humidity conditions.

## 3.2 Impact of dust transport on PM<sub>2.5</sub> chemical composition

On January 10, 2021, an extensive and intense dust storm, driven by successive cold fronts and sustained high-velocity winds, swept across northern China, triggering a dramatic surge in PM<sub>2.5</sub> concentrations (Fig. S3). At the foot of Mount Hua, PM<sub>2.5</sub> concentrations rapidly rose from 95  $\mu$ g m<sup>-3</sup> to 457  $\mu$ g m<sup>-3</sup> within 24 hours, reaching 3.4 times the non-dust average (127 ± 48  $\mu$ g m<sup>-3</sup>). Concurrently at the top, PM<sub>2.5</sub> climbed from 46 to 165  $\mu$ g m<sup>-3</sup>, representing a 5.9-fold rise compared to typical conditions (28 ± 14  $\mu$ g m<sup>-3</sup>). The cleaner atmospheric environment at the top amplified the relative impact of dust transport, while at the foot, existing local pollution partially masked the dust contribution. This contrast highlights the altitude-dependent response to dust events, with the top showing greater sensitivity due to its lower background pollution levels.

HYSPLIT trajectory analysis revealed the dust originated from the Inner Mongolia-Gansu arid region and was transported along a northwest path to the study area (Fig. S4). Dust transport was closely linked to atmospheric circulation, especially in the troposphere, where changes in wind speed play a key role in dust dispersion (Yang et al., 2017). During the dust period, wind speeds at the foot increased from 2.0 to 5.3 m s<sup>-1</sup>, and high-altitude wind speeds reached 12.2 m s<sup>-1</sup>, significantly higher than the average wind speed during non-dust periods  $(5.4 \pm 3.0 \text{ m s}^{-1})$ .

Although PM<sub>2.5</sub> absolute concentrations rose during the dust period, component concentration changes at the two sites differed markedly. At the foot of the Mount Hua, elemental carbon (EC) concentrations remained relatively stable (4.5  $\pm$  2.1 during non-dust vs. 4.8  $\pm$  1.8  $\mu$ g m<sup>-3</sup> during dust; Table S2). Organic carbon (OC) showed a modest increased from

 $17 \pm 8.0$  to  $19 \pm 4.6$  µg m<sup>-3</sup>, but its mass fraction in PM<sub>2.5</sub> decreased substantially from 13.4% to 4.4%, reflecting the overwhelming contribution of mineral dust. The top exhibited significantly different characteristics, with both EC and OC concentrations doubling from 0.9 to 1.8 µg m<sup>-3</sup> and 4.7 to 9.4 µg m<sup>-3</sup> respectively. OC maintained a higher mass fraction of 6.5% compared to 4.4% at the foot. These patterns indicate efficient mixing of dust with anthropogenic carbonaceous aerosols during long-range transport, coupled with more vigorous secondary formation processes in the free troposphere (Wang et al., 2023; Zheng et al., 2024). The elevated OC fraction at higher altitudes likely results from enhanced photochemical reactions and gas particle conversions under these atmospheric conditions.

Concentrations of mineral components like calcium and magnesium ions (Ca<sup>2+</sup> and Mg<sup>2+</sup>) rose significantly (foot: 1.8 to 7.7 μg m<sup>-3</sup>; top: 0.7 to 3.2 μg m<sup>-3</sup>), confirming their established role as reliable tracers of dust emissions (Li et al., 2016; Liu et al., 2024). SO<sub>4</sub><sup>2-</sup> concentrations also increased significantly at both sites (foot: 5.8 to 10.0 μg m<sup>-3</sup>; top: 3.8 to 8.7 μg m<sup>-3</sup>). This increase can be attributed to both the release of inherent sulfate species in dust (e.g., CaSO<sub>4</sub>) (Wu et al., 2012) was mainly due to and heterogeneous chemical reactions on dust particle surfaces, with where transition metals like such as Fe (III) and Mn (II) act as catalysts to promote catalyze the conversion of atmospheric sulfur dioxide (SO<sub>2</sub>) to SO<sub>4</sub><sup>2-</sup> (Harris et al., 2013; Myriokefalitakis et al., 2022).

Dust transport significantly altered the concentrations and molecular distribution of diacids and their precursors. Although  $C_2$  remained the most concentrated acidic molecule during dust periods, its absolute concentration decreased noticeably. At the foot of Mount Hua,  $C_2$  concentrations dropped from  $674 \pm 528$  ng m<sup>-3</sup> (non-dust periods) to  $276 \pm 20$  µg m<sup>-3</sup> (dust periods), a decrease of by 59%. At the top of Mount Hua,  $C_2$  concentrations decrease from  $306 \pm 204$  ng m<sup>-3</sup> to  $229 \pm 45$  ng m<sup>-3</sup>, a reduction of 25%. Severe ozone (O<sub>3</sub>) pollution was present in this dust storm event, and the particulate eruption promoted the generation and dispersion of O<sub>3</sub> pollutants. O<sub>3</sub> concentrations at the foot increased sharply from 15 µg m<sup>-3</sup> to 62 µg m<sup>-3</sup> (Fig. S3), much higher than the non-dust average of  $26 \pm 19$  µg m<sup>-3</sup>. The dust's dust's extinction effect likely reduced aerosol optical thickness, enhancing surface

UV radiation. Combined with a local temperature rise ( $\Delta T = +5.8^{\circ}C$ ), this probably triggered free-radical chain reactions, promoting the heterogeneous oxidation of  $C_2$  on mineral surfaces (Usher, et al., 2003; Lu et al., 2023; Usher, et al., 2003). Notably, the proportion of  $C_2$  in total diacids exhibited contrasting showed different trends at the two sites, decreasing from 37.3% to 32.2% at the foot and increasing from 35.5% to 42.8% at the top (Fig. 4c). This divergence could be closely related to the humidity levels at the two sites. During the dust events, the lower relative humidity at the foot experienced low relative humidity (RH =  $24 \pm 8.5\%$ ); suppressed inhibiting aqueous liquid-phase oxidation, whereas while the higher humidity at altitude the top (RH =  $44 \pm 11\%$ ) favored secondary— $C_2$  formation through such reactions. Additionally, variations in aerosol sources, transport pathways, aging processes, and potential contributions from other chemical reactions may also have influenced  $C_2$  generation.

As a major atmospheric keto acid and key precursor of C<sub>2</sub> (Kawamura et al., 2012; 2013), ωC<sub>2</sub> ranked second among the acids detected at both sites during non-dust periods, with concentrations of 214  $\pm$  199 ng m<sup>-3</sup> at the foot and 77  $\pm$  52 ng m<sup>-3</sup> at the top of Mount Hua. However, during dust periods, mGly became the second most abundant acid at both sites due to its enrichment on dust-particle surfaces. At the foot, mGly concentration reached  $116 \pm 34$ ng m<sup>-3</sup> (13.6% of total diacids), up from 5.9% in non-dust periods. At the top, mGly concentration was  $38 \pm 9$  ng m<sup>-3</sup> (7.1% of total diacids) (Fig. 4b), slightly higher than the nondust 5.6%. Phthalic acid (Ph), a photo-oxidation product of naphthalene and other aromatic hydrocarbons, primarily originates from industrial processes and incomplete combustion of coal in heavy and diesel vehicles (Ho et al., 2006). At both foot and top of Mount Hua, the proportion of Ph remains relatively stable, accounting for approximately 4% during both dust and non-dust periods, indicating that its sources are stable and closely related to regional industrial activities and traffic emissions. During dust periods, the C<sub>2</sub>/C<sub>4</sub> ratios at the foot and top of Mount Hua rose to 5.24 and 7.75 (Fig. 4c), showing stronger aerosol aging. However, the C<sub>3</sub>/C<sub>4</sub> ratio at top of Mount Hua dropped to 0.70, this might result from the combined effects of selective adsorption of C2 onto dust particles and enhanced photolysis of C<sub>3</sub> on mineral dust surfaces.

## 3.3 Size distribution characteristics of diacids and related compounds during non-dust and dust periods

During non-dust periods, the size distribution of  $C_2$  at both the foot and top of Mount Hua exhibitsed a distinct bimodal distributionpattern (Fig. 5a and 5(a)), characterized by a primarymajor peak in the fine particle mode (0.4-1.1 µm) and a secondary minor peak in the coarse particle mode (4.7-5.8 µm). Fine particles, with their greater specific surface area and hygroscopic nature, provide a conducive liquid-phase environment that enhances the oxidation of precursors such as mGly and Pyr, leading to  $C_2$  formation (Ervens et al., 2011; Wang et al., 2015). The high correlation between  $C_2$  and secondary inorganic ions ( $SO_4^{2-}$ ,  $NO_3^-$ ,  $NH_4^+$ ) (with  $R^2$  values of 0.92-0.95 at the foot and 0.48-0.92 at the top, p < 0.01; as shown in Fig. 6) supports this mechanism, confirming that  $C_2$  formation during non-dust periods primarily relies on liquid-phase oxidation reactions on fine particle surfaces. The lower  $R^2$  values at the top may be due to the greater influence of long-range transport at high-altitude sites, resulting in more complex sources of precursors.  $C_2$  in the coarse particle mode likely originates from direct adsorption of biogenic emissions (such as plant waxes) or heterogeneous oxidation of gasphase precursors on mineral dust surfaces (Wang et al., 2012).

The distribution patterns of short-chain diacids, such as C<sub>3</sub> and C<sub>4</sub> are similar to that of C<sub>2</sub> (Fig. 5b-c and 5(b)-(c)), with primarymain peaks at 0.4-1.1 μm and secondary peaks at 4.7-5.8 μm, indicating that these acids mainly come from fine particles. In contrast, glutaric (C<sub>5</sub>) acid shows distinct distribution characteristics at the two sites. At the foot, it exhibits a unimodal distribution single peak— in the coarse particles (4.7-5.8 μm) (Fig. 5d), while at the top, it displays a bimodal distribution (0.4-1.1 μm and 4.7-5.8 μm) (Fig. 5(d)). This significant difference in modal structure suggests that different atmospheric processes govern the behavior of C<sub>5</sub> at different altitudes. The C<sub>5</sub>-at the foot likely mainly comes from local emissions (Hatakeyama et al., 1985), such as the oxidation of cyclopentene in vehicle exhaust, whereas the high altitude area is influenced by a combination of long range transport and local processes (Zhao and Fu, 2018). Adipic (C<sub>6</sub>) acid shows a bimodal distribution at both sites, probably resulting from the oxidation of cyclohexene (in the fine mode) or adsorption of gas-

phase precursors on coarse particle surfaces (Deshmukh et al., 2016). Azelaic (C<sub>9</sub>) acid is significantly enriched only in fine particles at the foot, which may be closely related to the oxidation of unsaturated fatty acids emitted from biomass burning in northern regions during winter (Deshmukh et al., 2016). The coarse particle fraction of Ph likely forms through gasphase adsorption, consistent with the strong adsorption characteristics of coarse particles reported by Kanellopoulos et al. (2021).

The particle size distributions of mGly (Fig. 5g and 5(g)) and  $\omega$ C<sub>2</sub> (Fig. 5j and 5(j)) showed remarkable consistency with that of C<sub>2</sub> (Fig. 5a and 5(a)), providing direct evidence that aqueous-phase oxidation serves as the predominant formation pathway for C<sub>2</sub>. Pyr exhibited distinct altitudinal variation in its distribution characteristics. At the top of Mount Hua, Pyr displayed a similar size distribution pattern to C<sub>2</sub>, indicating their shared photochemical origin. In contrast, at the foot, Pyr demonstrated significant enrichment in coarse particles (4.7-5.8 µm), likely attributable to heterogeneous reactions of gaseous precursors from local coal combustion on mineral dust surfaces. Gly also exhibits a peak in coarse particles, likely due to its strong adsorption and chemical stability on particle surfaces. The diacids concentrations are consistently lower at the top compared to the foot, which is closely tied to substantial local emissions at the lower elevation. As shown in Fig. 6, the coal combustion and biomass burning tracer Cl<sup>-</sup> demonstrates an exceptionally strong correlation with C<sub>2</sub> (R<sup>2</sup> = 0.88, p< 0.01) at the foot.

The dust transport process significantly impacted the size distributions altered the particle size distribution characteristics of diacids in aerosols (Fig. 5). At the foot of the mountain, the C₂ concentration in fine particles (≤2.1 µm) decreased markedly from 8662 ng m<sup>-3</sup> to 4880 ng m<sup>-3</sup> (a reduction of 43.7% reduction) during dust events, while the concentration in coarse particle (>2.1 µm) concentration showed a modest increased from 2718 ng m<sup>-3</sup> to 2843 ng m<sup>-3</sup> (an increase of 4.6%) (Table 3). A more pronounced change was observed at the high-altitude top of Mount Hua, where the C₂ concentration in coarse particles (2301 ng m<sup>-3</sup>) exceeded that in fine particles (2161 ng m<sup>-3</sup>) during dust events, indicating a shift in the dominant particle size distribution from fine to coarse modes. This shift in particle size distribution can be

attributed to the formation of Ca(NO<sub>3</sub>)<sub>2</sub> coatings resulting from the reaction between calcium carbonate and NO<sub>3</sub><sup>-</sup> during dust aging (Li and Shao, 2009; Zhi et al., 2025). These hygroscopic coatings create favorable conditions for the adsorption and oxidation of gaseous organic compounds, thereby promoting the formation of SOA on the surfaces of coarse particles. Research by Li et al. (2025) further confirms that aqSOA formed on dust surfaces can effectively enhance SOA production and drive a transition in the size distribution from the submicron to the supermicron range, which is highly consistent with the observational results of this study. Size-segregated ion data (Fig. S5) provide direct evidence for the above mechanism. Ca<sup>2+</sup> was primarily present in the coarse mode (3.3–5.8 µm), while during dust events, NO<sub>3</sub><sup>-</sup> at the top migrated from the fine mode (0.4–1.1 µm) to the coarse mode (3.3–5.8 μm) and coexisted with Ca<sup>2+</sup> in the same size range, strongly supporting the formation of Ca(NO<sub>3</sub>)<sub>2</sub> coatings on dust particle surfaces. In contrast, at the foot of the mountain, although the concentration of NO<sub>3</sub><sup>-</sup> decreased, it remained predominantly in the fine mode. This spatial difference may stem from more thorough aging and reactions of aerosols at the top due to longer transport times. Meanwhile, the foot is influenced by local pollution, resulting in higher background NO<sub>3</sub><sup>-</sup> concentrations and competitive reactions with components such as SO<sub>4</sub><sup>2-</sup>, which may collectively delay the distinct shift of NO<sub>3</sub><sup>-</sup> to the coarse mode. These findings show excellent agreement with the research results of Li et al. (2025), which demonstrated that calcium carbonate reacts with nitric acid during dust aging processes to form calcium nitrate (Ca(NO<sub>3</sub>)<sub>2</sub>). The resulting hygroscopic surfaces provide favorable conditions for the adsorption and heterogeneous oxidation of gaseous organic compounds. Furthermore, aqueous secondary organic aerosols (aqSOA) formed on dust surfaces promote SOA formation and drive the transition of particle size distribution from submicron to supermicron ranges.

453

454

455

456

457

458

459

460

461

462

463

464

465

466

467

468

469

470

471

472

473

474

475

476

477

478

479

480

Analysis of the dust/non-dust concentration ratio  $(R_D/N)$  revealed  $R_D/N$  values of 0.3 and 0.6 for fine and coarse particles at the foot, respectively, while these values reached 0.4 and 1.1 at the top, indicating that dust processes have a more significant-impact on the particle size distribution of diacids at high-altitude regions. Further investigations confirmed significant enrichment of  $C_2$  precursors (mGly, Pyr, and  $\omega C_2$ ) in the coarse particle fraction (>2.1  $\mu$ m).

Observational data from the top of Mount Hua revealed that the concentration ratio ( $R_{D/N}$ ) of these precursors in coarse particles during dust periods reaches 0.8-1.4 during dust periods, higher than the 0.5-0.7 ratio in fine particles ( $\leq$ 2.1 µm), demonstrating the crucial contribution of heterogeneous oxidation on dust particle surfaces to  $C_2$  formation. Throughout dust episodes, the particle size distribution patterns of diacids ( $C_2$ - $C_6$ ) consistently displayed a pronounced shift from fine to coarse particles (4.7-5.8 µm) (Fig. 5). Notably, concentrations of the biomass burning tracer  $C_9$  decreased during dust episodes, while Ph and isophthalic acid (iPh) showed distinct peaks in the coarse particle mode. This phenomenon indicates that dust particles effectively scavenge gaseous pollutants through strong adsorption, thereby suppressing the formation of local fine-mode secondary organic aerosols (SOA). However, these gaseous precursors adsorbed onto coarse particle surfaces can still undergo heterogeneous oxidation reactions to form SOA.

During dust events, the correlation between C<sub>2</sub> and mineral ions (Ca<sup>2+</sup>, Mg<sup>2+</sup>) showed significant enhancement (with R<sup>2</sup> values of 0.33-, 0.30; p<0.05 at the foot and 0.65-, 0.39; p<0.01 at the top). This finding showsed excellent agreement with the recent research results of Li et al. (2025), who similarly observed stronger correlations between Ca<sup>2+</sup> and oxalateC<sub>2</sub>  $(R^2=0.46-0.95)$  in the coarse particle phase. This arises as organic acids like  $\frac{\text{oxalic acid} C_2}{\text{oxalic acid}}$  in aged carbonate-containing dust particles react with carbonates to form stable salts (Ervens et al., 2008; Lim et al., 2010). This process inhibits the volatility of organic acids and stabilizes them in the coarse particle phase. Furthermore, due to differences in rock types and weathering processes, Asian dust particles inherently contain higher concentrations of alkaline metal elements (Ca and Mg) compared to dust from other regions (Yu et al., 2025). The size-resolved correlations between C<sub>2</sub>, Ca<sup>2+</sup>, and Mg<sup>2+</sup> (Fig. 6), further support this conclusion. During dust events, the concentrations of C2, Ca2+, and Mg2+ exhibited synchronous increases with increasing particle size. In contrast, during non-dust periods, the peak concentration of C<sub>2</sub> occurred in the fine particle size range, while mineral ion concentrations did not show corresponding increases. As described in Section 3.2, dust events led to significant reductions in  $C_2$  concentrations in  $PM_{2.5}$  (foot:  $674 \pm 528$  ng m<sup>-3</sup> during non-dust periods vs.  $276 \pm 20$  ng  $m^{-3}$  during dust periods; top:  $306 \pm 204$  ng  $m^{-3}$  during non-dust periods vs.  $229 \pm 45$  ng  $m^{-3}$  during dust periods).

Overall, the transformation mechanisms of C<sub>2</sub> and its precursors underwent significant alterations during dust events, shifting from aqueous-phase oxidation dominated in fine particles during non-dust periods to heterogeneous oxidation on coarse particle surfaces as the primary pathway during dust episodes. Regional comparative analysis further revealed that atmospheric chemical processes at the mountain foot were mainly influenced by local emission sources such as coal combustion and biomass burning, whereas the summit site more clearly reflected the complex interactions between long-range dust transport and regional atmospheric processes.

### 3.4 Stable carbon isotopes ( $\delta^{13}$ C) of oxalic acid

Synchronized observations at the foot and top of Mount Hua (2060 m asl) revealed an inverse correlation between  $C_2$  concentration and  $\delta^{13}$ C values in PM<sub>2.5</sub> (Fig. 7a and 7b). When  $C_2$  concentration at the foot increased to 2424 ng m<sup>-3</sup>, its  $\delta^{13}$ C value decreased to -34.5‰, while at the top, a concentration of 917 ng m<sup>-3</sup> corresponded to a  $\delta^{13}$ C of -24.7‰. Conversely, during low concentration periods,  $\delta^{13}$ C at the foot rose to -21.9‰ (258 ng m<sup>-3</sup>) and at the top to -17.2‰ (63 ng m<sup>-3</sup>). This systematic variation provides clear evidence for significant kinetic carbon isotope fractionation during atmospheric aqueous-phase oxidation processes. Specifically, volatile organic compounds (VOCs) and semi-volatile organic compounds (SVOCs) with lower  $\delta^{13}$ C values preferentially react to form aqSOA, resulting in  $^{13}$ C-depleted products (Xu et al., 2022).

Spatially, the  $\delta^{13}$ C values of  $C_2$  in PM<sub>2.5</sub> at the top of Mount Hua (-28.4‰ to -12.8‰, mean -21.5‰) were significantly higher than those at the foot (-36.2‰ to -14.9‰, mean -27.6‰). This vertical gradient primarily results from long-range transport of aerosols at high altitudes coupled with deep oxidation processes. The higher  $C_2/C_4$  ratio observed at Mount Hua (5.84 vs. 4.74 at the foot) indicates more pronounced atmospheric aging characteristics. This distribution pattern originates from prolonged photochemical oxidation during long-range transport, where preferential cleavage of  $^{12}$ C- $^{12}$ C bonds (due to their lower bond energy) leads

to relative  $^{13}$ C enrichment in residual  $C_2$ . In contrast, surface aerosols dominated by local fresh emissions undergo shorter oxidation periods and exhibit weaker isotope fractionation effects. Moreover,  $\delta^{13}$ C can provide insights into the sources of aerosols, Pavuluri and Kawamura (2016) found that biogenic aerosols had higher mean  $\delta^{13}$ C values (-15.8‰) than anthropogenic sources (-19.5‰). Our study shows that foot aerosols were mainly influenced by anthropogenic sources (biomass burning and coal combustion), while the top was more affected by natural sources due to richer vegetation, with long-range transport potentially weakening local isotope fractionation effects.

During dust events, C<sub>2</sub> concentrations in PM<sub>2.5</sub> showed significant decreasing trends, declining from  $674 \pm 528$  ng m<sup>-3</sup> to  $276 \pm 20$  ng m<sup>-3</sup> at the foot and from  $306 \pm 204$  ng m<sup>-3</sup> to  $229\pm45~\text{ng}~\text{m}^{-3}$  at the top of Mount Hua. Concurrently, the  $\delta^{13}C$  values of  $C_2$  exhibited distinct positive shifts, increasing from -27.6% to -23.9% at the foot and from -21.5% to -13.2% at the top. This phenomenon reveals key chemical transformation mechanisms during dust transport: alkaline mineral surfaces promote heterogeneous catalytic oxidation of oxalate-C2 precursors, with coarse-mode mineral components (Ca<sup>2+</sup>/Mg<sup>2+</sup> etc.) preferentially combining with <sup>13</sup>C-labeled C<sub>2</sub> to form stable compounds like calcium oxalate. This mechanism is strongly supported by observational data during dust events, both oxalic acid and Ca<sup>2+</sup>/Mg<sup>2+</sup> concentrations showed significant increases with growing particle size, while exhibiting high correlations ( $R^2 = 0.30-0.65$ ) during dust periods. Simultaneously, <sup>12</sup>C-enriched C<sub>2</sub> produced on fine particle surfaces moves to coarse particles through gas-particle conversion or coagulation, resulting in <sup>13</sup>C-enriched residues remaining in fine particles. As demonstrated by the aforementioned research findings, the concentration of oxalic acid in coarse particles showed a marked increase during dust events, with this variation being particularly pronounced at the top. These two synergistic processes collectively altered both aerosol size distribution and isotopic composition characteristics.

## 4. Conclusions

537

538

539

540

541

542

543

544

545

546

547

548

549

550

551

552

553

554

555

556

557

558

559

560

561

562

563

564

This study provides compelling evidence for the dual role of dust transport in modulating oxalic acid formation and isotopic composition in atmospheric aerosols. Through

comprehensive analysis of PM<sub>2.5</sub> and size-segregated samples, we demonstrate that dust events trigger a fundamental shift in oxalic acid production pathways from predominant aqueous-phase oxidation in fine particles during non-dust periods (showing strong humidity dependence below 75% RH) to mineral heterogeneous chemistry in coarse particles during dust episodes (Fig. 8). The dust induced transformations are particularly pronounced at high-altitude sites like Mount Hua, where we observed: (1) enhanced aerosol aging indicators ( $C_2/C_4$  ratio increasing to 7.75); (2) significant  $\delta^{13}$ C enrichment (+8.3% compared to non-dust periods); and (3) preferential partitioning of C<sub>2</sub>oxalate to coarse-mode particles (coarse/fine particle ratio reaching 1.1). These changes result from synergistic effects of surface-catalyzed oxidation favoring  $^{13}$ C retention and metal-oxalate complexation. Conversely, surface sites exhibited stronger local anthropogenic influences, with higher C<sub>2</sub>oxalate concentrations (674 ± 528 ng m<sup>-3</sup>) but lower  $\delta^{13}$ C values (-27.6%), reflecting less processed aerosols. The identified inverse oxalateC<sub>2</sub>- $\delta^{13}$ C relationship and altitude-dependent response to dust transport provide new quantitative tools for evaluating aerosol aging processes and improving regional air quality models, particularly in dust-prone regions under changing climate conditions.

### **Data availability**

The data in this study are available at <a href="https://zenodo.org/doi/10.5281/zenodo.15788834">https://zenodo.org/doi/10.5281/zenodo.15788834</a> (Shen et al., 2025).

### **Author contributions**

Jianjun Li conceived and designed the study. Minxia Shen conducted the literature search, performed sample and data analysis, and wrote the manuscript. Jianjun Li and Qiyuan Wang contributed to manuscript revision. Weining Qi, Yali Liu, Yifan Zhang, Wenting Dai, Lu Li, Xiao Guo, Yue Cao, Yingkun Jiang, Qian Wang and Shicong Li collected particulate samples and supervised the experiments. All authors provided critical feedback on the manuscript and approved the final version.

### **Conflict of Interest**

The authors declare no conflicts of interest relevant to this study.

### Acknowledgments

592

- This work was jointly supported by the program from National Natural Science
- Foundation of China (No. 42407156), State Key Laboratory of Loess and Quaternary Geology
- 595 (SKLLOG2307), and the Natural Science Basic Research Program of Shaanxi Province
- 596 (2025JC-YBQN-450). Jianjun Li also acknowledged the support of the Youth Innovation
- 597 Promotion Association Chinese Academy of Sciences (No. 2020407).

### 598 References

- Bikkina, P., Bikkina, S., and Kawamura, K.: Role of aerosol liquid water content on the production of
- dicarboxylic acids in the dust-laden air masses over the Arabian Sea: Implications for heterogeneous
- 601 chemistry. Atmos. Res., 289, 106743. <a href="https://doi.org/10.1016/j.atmosres.2023.106743">https://doi.org/10.1016/j.atmosres.2023.106743</a>, 2023.
- 602 Cao, J. J., Lee, S. C., Chow, J. C., Watson, J. G., Ho, K. F., Zhang, R. J., Jin, Z. D., Shen, Z. X., Chen, G. C.,
- Kang, Y. M., Zou, S. C., Zhang, L. Z., Qi, S. H., Dai, M. H., Cheng, Y. and Hu. K.: Spatial and seasonal
- distributions of carbonaceous aerosols over China, J. Geophys. Res. Atmos., 112(D22), D22S11,
- 605 <u>https://doi.org/10.1029/2006JD008205</u>, 2007.
- 606 Carlton, A. G., Turpin, B. J., Lim, H. J., Altieri, K. E., and Seitzinger, S.: Link between isoprene and
- 607 secondary organic aerosol (SOA): Pyruvic acid oxidation yields low volatility organic acids in clouds,
- 608 Geophy. Res. Lett., 33, L06822, https://doi.org/10.1029/2005GL025374, 2006.
- 609 Chen, J. C., Xu, J. Z., Wu, Z. J., Meng, X. X. Y., Yu, Y., Ginoux, P., DeMott, P. J., Xu, R., Zhai, L. X., Yan,
- Y. F., Zhao, C. F., Li, S. M., Zhu, T., and Hu, M.: Decreased dust particles amplify the cloud cooling effect
- by regulating cloud ice formation over the Tibetan Plateau. Sci. Adv. 10(37), eado0885.
- 612 <a href="https://doi.org/10.1126/sciadv.ado0885">https://doi.org/10.1126/sciadv.ado0885</a>, 2024.
- 613 Chen, S. Y., Zhao, D., Huang, J. P., He, J. Q., Chen, Y., Chen, J. Y., Bi, H. R., Lou, G. T., Du, S. K., Zhang,
- Y., and Yang, Fan.: Mongolia contributed more than 42% of the dust concentrations in Northern China in
- March and April 2023. Adv. Atmos. Sci., 40(9), 1549–1557. <a href="https://doi.org/10.1007/s00376-023-3062-1">https://doi.org/10.1007/s00376-023-3062-1</a>,
- 616 2023.
- 617 Deguillaume, L., Leriche, M., Desboeufs, K., Mailhot, G., George C., and Chaumerliac, N.: Transition
- 618 metals in atmospheric liquid phases: sources, reactivity, and sensitive parameters. Chem. Rev., 105(9), 3388
- 619 3431. https://doi.org/10.1021/cr040649c, 2005.

- 620 Deshmukh, D. K., Kawamura, K., and Deb, M. K.: Dicarboxylic acids, ω-oxocarboxylic acids, α-
- dicarbonyls, WSOC, OC, EC, and inorganic ions in wintertime size-segregated aerosols from central
- 622 India: Sources and formation processes. Chemosphere, 161, 27–42.
- 623 <u>https://doi.org/10.1016/j.chemosphere.2016.06.107</u>, 2016.
- 624 Deshmukh, D. K., Kawamura, K., Deb, M. K., and Boreddy, S. K. R.: Sources and formation processes of
- water-soluble dicarboxylic acids, ω-oxocarboxylic acids, α-dicarbonyls, and major ions in summer aerosols
- 626 from eastern central India. J. Geophys. Res. Atmos., 122(6), 3630-3652.
- 627 <u>https://doi.org/10.1002/2016JD026246</u>, 2017.
- 628 Du, W., Ding, Z. J., Lei, Y. L., Zhang, S., Wu, C., Zhang, F., Wang, F. L., Lv, S. J., Liu, X. D., Meng, J. J.,
- and Wang, G. H.: Atmospheric fine particulate dicarboxylic acids and related SOA in winter at the
- background site of Yangtze River Delta: Implication for the long-distance transport of solid fuels burning.
- 631 Atmos. Environ. 289, 11932. https://doi.org/10.1016/j.atmosenv.2022.119320, 2022.
- 632 Ervens, B., Turpin, B. J., and Weber, R. J.: Secondary organic aerosol formation in cloud droplets and
- aqueous particles (aqSOA): a review of laboratory, field and model studies. Atmos. Chem. Phys., 11(21),
- 634 11069–11102. <a href="https://doi.org/10.5194/acp-11-11069-2011">https://doi.org/10.5194/acp-11-11069-2011</a>, 2011.
- 635 Falkovich, A. H., and Schkolnik, G.: Adsorption of organic compounds pertinent to urban environmentsonto
- 636 mineral dust particles. J. Geophys. Res. Atmos., 109, D02208. https://doi.org/10.1029/2003JD003919, 2004.
- 637 Fan, J. Y., Wang, Y., Rosenfeld, D., and Liu, X. H.: Review of aerosol-cloud interactions: Mechanisms,
- 638 significance, and challenges. J. Atmos. Sci., 73(11), 4221–4252. https://doi.org/10.1175/JAS-D-16-0037.1,
- 639 2016.
- 640 Fountoukis, C., and Nenes, A.: ISORROPIA II: a computationally efficient thermodynamic equilibrium
- model for  $K^+$ -Ca<sup>2+</sup>-Mg<sup>2+</sup>-NH4<sup>+</sup>-Na<sup>+</sup>-SO<sub>4</sub><sup>2-</sup>-NO<sub>3</sub><sup>-</sup>-Cl<sup>-</sup>-H<sub>2</sub>O aerosols. Atmos. Chem. Phys., 7(17), 4639–4659.
- 642 https://doi.org/10.5194/acp-7-4639-2007, 2007.
- 643 Fu, P. Q., Kawamura K., Kanaya, Y., and Wang, Z. F.: Contributions of biogenic volatile organic compounds
- 644 to the formation of secondary organic aerosols over Mt. Tai, Central East China. Atmos. Environ., 44, 4817–
- 645 <u>4826. https://doi.org/10.1016/j.atmosenv.2010.08.040, 2010.</u>
- 646 Fu, T. M., Jacob, D. J., Wittrock, F., Burrows, J. P., Vrekoussis, M., and Henze, D. K.: Global budgets of
- atmospheric glyoxal and methylglyoxal, and implications for formation of secondary organic aerosols. J.

- Geophys. Res. 113. D15303, https://doi.org/15310.11029/12007JD009505, 2008.
- 649 Gui, K., Yao, W. R., Che, H. Z., An, L.C., Zheng, Y., Li, L., Zhao, H. J., Zhang, L., Zhong, J. T., Wang, Y.
- Q., and Zhang, X.Y.: Record-breaking dust loading during two mega dust storm events over northern China
- in March 2021: aerosol optical and radiative properties and meteorological drivers. Atmos. Chem. Phys.
- 652 22(12), 7905–7932. https://doi.org/10.5194/acp-22-7905-2022, 2022.
- Harris, E., Bärbel Sinha, van Pinxteren, D., Tilgner, Andreas., Fomba, K. W., Schneider, J., Roth, A., Gnauk,
- T., Fahlbusch, B., Mertes, S., Lee, T., Collett, J., Foley, S., Borrmann, S., Hoppe, P., and Herrmann, H.:
- Enhanced role of transition metal ion catalysis during in-cloud oxidation of SO<sub>2</sub>. Science, 340(6133),727–
- 656 730. https://doi.org/10.1126/science.123091, 2023.
- 657 Hatakeyama, S., Ohno, M., Weng, J., Takagi, H., and Akimoto, H.: Mechanism for the formation of gaseous
- and particulate products from ozone-cycloalkene reactions in air, Environ. Sci. Technol., 21, 52-57,
- 659 <u>https://doi.org/10.1021/es00155a005, 1987.</u>
- 660 Huang, R. J., Li, Y. J., Chen, Q., Zhang, Y. L., Lin, C. S., Chan, C. K., Yu, J. Z., Gouw, J., Tong, S. R., Jiang,
- J. K., Wang, W. G., Ding, X., Wang, X. M., Ge, M. F., Zhou, W. J., Worsnop, D., Boy, M., Bilde, M., Dusek,
- 662 <u>U., Carlton, A. G., Hoffmann, T., McNeill, V. F., and Glasius M.: Secondary organic aerosol in urban China:</u>
- A distinct chemical regime for air pollution studies, Science, 389, eadq2840. https://doi.org/
- 664 <u>10.1126/science.adq2840, 2025.</u>
- Ho, K. F., Lee, S. C., Cao, J. J., Kawamura, K., Watanabe, T., Cheng, Y., and Chow, J. C.: Dicarboxylic acids,
- ketocarboxylic acids and dicarbonyls in the urban roadside area of Hong Kong, Atmos. Environ., 40, 3030–
- 667 3040, https://doi.org/10.1016/j.atmosenv.2005.11.069, 2006.
- 668 Hoque, M. M., Kawamura, K., and Uematsu, M.: Spatio temporal distributions of dicarboxylic acids, ω
- 669 -oxocarboxylic acids, pyruvic acid, α-dicarbonyls and fatty acids in the marine aerosols from the North and
- 670 South Pacific, Atmos. Res., 185, 158–168, https://doi.org/10.1016/j.atmosres.2016.10.022, 2017.
- Kalogridis, A. C., Popovicheva, O. B., Engling, G., Diapouli, E., Kawamura, K., Tachibana, E., Ono, K.,
- 672 Kozlov, V. S., and Eleftheriadis. K.: Smoke aerosol chemistry and aging of Siberian biomass burning
- 673 emissions in a large aerosol chamber. Atmos. Environ. 185, 15–28.
- https://doi.org/10.1016/j.atmosenv.2018.04.033, 2018.
- Kanellopoulos, P. G., Chrysochou, E., Koukoulakis, K., and Bakeas E.: Secondary organic aerosol markers
- and related polar organic compounds in summer aerosols from a sub-urban site in Athens: Size distributions,

- 677 diurnal trends and source apportionment. Atmos. Pollut. Res., 12, 1-13.
- 678 <u>https://doi.org/10.1016/j.apr.2021.02.01</u>, 2021.
- Kawai, K., Matsui, H., and Tobo, Y.: High potential of Asian dust to act as ice nucleating particles in mixed-
- phase clouds simulated with a global aerosol-climate model. J. Geophys. Res. Atmos., 126(12),
- 681 e2020JD034263. https://doi.org/10.1029/2020JD034263, 2021.
- 682 Kawamura, K., and Bikkina, S.: A review of dicarboxylic acids and related compounds in atmospheric
- 683 aerosols: Molecular distributions, sources and transformation. Atmos. Res., 170(15), 140-160.
- 684 <u>https://doi.org/10.1016/j.atmosres.2015.11.018</u>, 2016.
- Kawamura, K., and Ikushima, K.: Seasonal changes in the distribution of dicarboxylic acids in the urban
- atmosphere, Environ. Sci. Technol., 27, 2227-2235, https://doi.org/10.1021/es00047a033, 1993.
- 687 Kawamura, K. and Sakaguchi, F.: Molecular distributions of water soluble dicarboxylic acids in marine
- aerosols over the Pacific Ocean including tropics, J. Geophys. Res.-Atmos., 104, 3501-3509,
- 689 <u>https://doi.org/10.1029/1998JD100041</u>, 1999.
- 690 Kawamura, K., and Watanabe, T.: Determination of stable carbon isotopic compositions of low molecular
- 691 weight dicarboxylic acids and ketocarboxylic acids in atmospheric aerosol and snow samples. Anal. Chem.,
- 692 76(19), 5762–5768. https://doi.org/10.1021/ac049491m, 2004.
- Kawamura, K., Ono, K., Tachibana, E., Charriére, B., and Sempéré, R.: Distributions of low molecular
- weight dicarboxylic acids, ketoacids and  $\alpha$ -dicarbonyls in the marine aerosols collected over the Arctic
- Ocean during late summer, Biogeosciences, 9, 4725–4737, <a href="https://doi.org/10.5194/bg-9-4725-2012">https://doi.org/10.5194/bg-9-4725-2012</a>, 2012.
- 696 Kawamura, K., Tachibana, E., Okuzawa, K., Aggarwal, S. G., Kanaya, Y., and Wang, Z. F.: High abundances
- of water-soluble dicarboxylic acids, ketocarboxylic acids and α-dicarbonyls in the mountaintop aerosols over
- 698 the North China Plain during wheat burning season, Atmos. Chem. Phys., 13, 8285–8302,
- 699 https://doi.org/10.5194/acp-13-8285-2013, 2013.
- Kok, J. F., Storelvmo, T., Karydis, V. A., Adebiyi, A. A., Mahowald, N. M., Evan, A.T., He, C. L., and Leung,
- D. M.: Mineral dust aerosol impacts on global climate and climate change. Nat. Rev. Earth Env., 4, 71–86-,
- 702 https://doi.org/10.1038/s43017-022-00379-5, 2023.
- Kumar, R., Barth, M. C., Madronich, S., Naja, M., Carmichael, G. R., Pfister, G. G., Knote, C., Brasseur, G.
- P., Ojha, N. and Sarangi, T.: Effects of dust aerosols on tropospheric chemistry during a typical pre-monsoon

- season dust storm in northern India. Atmos. Chem. Phys., 14, 6813–6834, 2014, https://doi.org/10.5194/acp-
- 706 <u>14-6813-2014</u>, 2014.
- 707 Kunwar, B. and Kawamura, K.: Seasonal distributions and sources of low molecular weight dicarboxylic
- 708 acids, v-oxocarboxylic acids, pyruvic acid, a-dicarbonyls and fatty acids in ambient aerosols from
- 709 subtropical Okinawa in the western Pacific Rim, Environ. Chem., 11, 673-689,
- 710 https://doi.org/10.1071/EN14097, 2014.
- 711 Lamkaddam, H., Dommen, J., Ranjithkumar, A., Gordon, H., Wehrle, G., Krechmer, J., Majluf, F., Salionov,
- 712 D., Schmale, J., Bjelić, S., Carslaw, K. S., Haddad, I. E., and Baltensperger, U.: Large contribution to
- 713 secondary organic aerosolfrom isoprene cloud chemistry. Sci. Adv., 7, eabe2952.
- 714 <u>https://doi.org/10.1126/sciadv.abe2952, 2021.</u>
- 715 Li, J. J., Wang, G. H., Ren, Y. Q., Wang, J. Y., Wu, C., Han, Y., Zhang, L., Cheng, C. L., and Meng, J. J.:
- 716 Identification of chemical compositions and sources of atmospheric aerosols in Xi'an, inland China during
- 717 two types of haze events. Sci. Total Environ., 566-567, 230-237.
- 718 <u>https://doi.org/10.1016/j.scitotenv.2016.05.057</u>, 2016.
- 719 Li, J., Wang, G. H., Zhang, Q., Li, J., Wu, C., Jiang, W. Q., Zhu, T., and Zeng, L. M.: Molecular
- 720 characteristics and diurnal variations of organic aerosols at a rural site in the North China Plain with
- 721 implications for the influence of regional biomass burning. Atmos. Chem. Phys., 19(16), 10481–10496,
- 722 https://doi.org/10.5194/acp-19-10481-2019, 2019.
- 723 Li, J. J., Wang, G. H., Zhou, B. H., Cheng, C. L., Cao, J. J., Shen, Z. X., and An, Z. S.: Airborne particulate
- 724 organics at the summit (2060 m, a.s.l.) of Mt. Hua in central China during winter: Implications for biofuel
- and coal combustion. Atmos. Res., 106,108–119, https://doi.org/10.1016/j.atmosres.2011.11.012, 2012.
- Li, W. J., and Shao L. Y.: Observation of nitrate coatings on atmospheric mineral dust particles. Atmos. Chem.
- 727 Phys., 9(6), 1863–1871. https://doi.org/10.5194/acp-10-10521-2010, 2009.
- 728 Li, W. J., Ito, A., Wang, G. C., Zhi, M. K., Xu, L., Yuan, Q., Zhang, J., Liu, L., Wu, F., Laskin, A., Zhang, D.
- 729 Z., Zhang, X.Y., Zhu, T., Chen, J. M., Mihalopoulos, N., Bougiatioti, A., Kanakidou, M., Wang, G. H., Hu,
- H. L., Zhao, Y., and Shi, Z. B.: Aqueous-phase secondary organic aerosol formation on mineral dust, Natl.
- 731 Sci. Rev., nwaf221, https://doi.org/10.1093/nsr/nwaf221, 2025.
- Liang, P., Chen, B., Yang, X. P., Liu, Q. Q., Li, A. R., Mackenzie, L., and Zhang, D. G.: Revealing the dust

- transport processes of the 2021 mega dust storm event in northern China. Sci. Bull., 67(1), 21-24.
- 734 <u>https://doi.org/10.1016/j.scib.2021.08.014</u>, 2022.
- 735 Lim, H. J., Carlton, A. G., and Turpin, B. J.: Isoprene forms secondary organic aerosol through cloud
- 736 processing: model simulations. Environ. Sci. Technol. 39(12), 4441–4446.
- 737 <u>https://doi.org/10.1021/es048039h, 2005.</u>
- 738 Lim, Y. B., Tan, Y., Perri, M. J., S. P. Seitzinger., and Turpin., B. J.: Aqueous chemistry and its role in
- 739 secondary organic aerosol (SOA) formation. Atmos. Chem. Phys., 10(21), 10521-10539.
- 740 <u>https://doi.org/10.5194/acp-10-10521-2010</u>, 2010.
- 741 Liu, H. J., Feng, Q., Huang, Y., Wu, F., Liu, Y. L., Shen, M. X., Guo, X., Dai, W. T., Qi, W. N., Zhang, Y. F.,
- Li, L., Wang, Q. Y., Zhou, B. H., and Li, J. J.: Composition and size distribution of wintertime inorganic
- aerosols at ground and alpine regions of northwest China. Chin. Chem. Lett., 35(11), 109636.
- 744 <u>https://doi.org/10.1016/j.cclet.2024.109636</u>, 2024.
- 745 Lu, Da., Li, H., Tian, M. K., Wang, G. C., Qin, X. F., Zhao, N., Huo, J. T., Yang, F., Lin, Y. F., Chen, J., Fu,
- Q. Y., Duan, Y. S., Dong, X.Y., Deng, C. R., Abdullaev, S. F., and Huang, K.: Secondary aerosol formation
- during a special dust transport event: impacts from unusually enhanced ozone and dust backflows over the
- 748 ocean. Atmos. Chem. Phys., 23(21), 13853–13868, https://doi.org/10.5194/acp-23-13853-2023, 2023.
- 749 Luo, Y. Y., Yao, Q., Ding, P., Hou, M., Deng, F. C., Wang, Y. B., Ding, C., Li, X., Wang, D. C., Sun, Z. k.,
- 750 Tang, S., Mao, Y. X., and Yao, X. Y.: Health impacts of an extreme dust event: a case and risk assessment
- study on airborne bacteria in Beijing, China. Environ. Sci. Eur., 36:41. https://doi.org/10.1186/s12302-024-
- 752 <u>00858-0</u>, 2024.
- Maher, B. A., Prospero, J. M., Mackie, D., Gaiero, D., Hesse P. P., and Balkanski Y.: Global connections
- between aeolian dust, climate and ocean biogeochemistry at the present day and at the last glacial maximum.
- 755 Earth Sci. Rev., 99(1–2), 61–97. https://doi.org/10.1016/j.earscirev.2009.12.001, 2010.
- Mahowald, N., Albani, S., Kok, J. F., Engelstaeder, S., Scanza, R., Ward, D. S., and Flanner, M. G.: The size
- 757 distribution of desert dust aerosols and its impact on the Earth system. Aeolian Res., 15, 53-71,
- 758 https://doi.org/10.1016/j.aeolia.2013.09.002, 2014.
- 759 Marx, S. K., Hooper, J., Irino, T., Stromsoe, N., Saunders, K. M., Seki, O., Dosseto, A., Johansen, A., Hua,
- Q., Dux, F., Jacobsen, G., and Zawadzki, A.: Atmospheric particulates over the northwestern Pacific during

- 761 the late Holocene: Volcanism, dust, and human perturbation. Sci. Adv. 10(43), eadn3311,
- 762 https://doi.org/10.1126/sciadv.adn3311, 2024.
- 763 Meng, J. J., Wang, G. H., Li, J. J., Cheng, C. L., Ren, Y. Q., Huang, Y., Cheng, Y. B., Cao, J. J., and Zhang,
- 764 <u>T.: Seasonal characteristics of oxalic acid and related SOA in the free troposphere of Mt. Hua, central China:</u>
- 765 Implications for sources and for mation mechanisms, Sci. Total Environ., 493, 1088–1097,
- 766 <u>https://doi.org/10.1016/j.scitotenv.2014.04.086, 2014.</u>
- 767 Meng, J. J., Wang, G. H., Hou, Z. F, Liu, X. D, Wei, B. J, Wu, C., Cao, C., Wang, J. Y., Li, J. J., Cao, J. J.,
- 768 Zhang, E., Dong, J., Liu, J. Z, Ge, S. S., and Xie, Y. N.: Molecular distribution and stable carbon isotopic
- 769 compositions of dicarboxylic acids and related SOA from biogenic sources in the summertime atmosphere
- of Mt. Tai in the North China Plain, Atmos. Chem. Phys., 18, 15069–15086, <a href="https://doi.org/10.5194/acp-18-">https://doi.org/10.5194/acp-18-</a>
- 771 <u>15069-2018</u>, 2018.
- 772 Mochida, M., Umemoto, N., Kawamura, K., and Uematsu, M.: Bimodal size distribution of C2-C4
- 773 dicarboxylic acids in the marine aerosols. Geophys. Res. Lett., 30(13), 1672
- 774 <u>https://doi.org/10.1029/2003GL017451, 2003.</u>
- 775 Myriokefalitakis, S., Tsigaridis, K., Mihalopoulos, N., Sciare, J., Nenes, A., Kawamura, K., Segers, A., and
- Kanakidou, M.: In-cloud oxalate formation in the global troposphere: a 3-D modeling study. Atmos. Chem.
- 777 Phys., 11(12), 5761–5782. https://doi.org/10.5194/acp-11-5761-2011, 2011.
- 778 Myriokefalitakis, S., Bergas-Massó, E., Gonçalves-Ageitos, M., García-Pando, C. P., Noije, T., Sager, P. L.,
- 779 Ito, A., Athanasopoulou, E., Nenes, A., Kanakidou, M., Krol, M. C., and Gerasopoulos, E.: Multiphase
- 780 processes in the EC-Earth model and their relevance to the atmospheric oxalate, sulfate, and iron cycles.
- 781 Geosci. Model Dev., 15(7), 3079–3120, <a href="https://doi.org/10.5194/gmd-15-3079-2022">https://doi.org/10.5194/gmd-15-3079-2022</a>, 2022.
- 782 Pan, H. Z., Hu, Z. Y., Feng, T. C., Huang, Z. W., Liu, Q. T., and Feng, G. L.: Distribution characteristics and
- 783 air-quality effect of intercontinental transport dust: An unexpected dust storm case study in China. Atmos.
- 784 Environ., 350, 121177. <a href="https://doi.org/10.1016/j.atmosenv.2025.121177">https://doi.org/10.1016/j.atmosenv.2025.121177</a>, 2025.
- 785 Pavuluri, C. M. and Kawamura, K.: Enrichment of <sup>13</sup>C in diacids and related compounds during
- photochemical processing of aqueous aerosols: New proxy for organic aerosols aging, Sci. Rep. UK, 6,
- 787 36467, https://doi.org/10.1038/srep36467, 2016.
- 788 Ponczek, M., Hayeck, N., Emmelin C., and George, C.: Heterogeneous photochemistry of dicarboxylic acids

- 789 on mineral dust. Atmos. Environ., 212, 262–271. https://doi.org/10.1016/j.atmosenv.2019.05.032, 2019.
- 790 Ren, Y. Q., Wang, G. H., Li, J. J., Wu, C., Cao, C., Li, J., Wang, J. Y., Ge, S. S., Xie, Y. N., Li, X. R., Meng,
- 791 F. and Li, H.: Evolution of aerosol chemistry in Xi'an during the spring dust storm periods: Implications for
- heterogeneous formation of secondary organic aerosols on the dust surface. Chemosphere, 215, 413–421.
- 793 https://doi.org/10.1016/j.chemosphere.2018.10.064, 2019.
- 794 Shen, M. X., Qi, W. N., Guo, X., Dai, W. T., Wang, Q. Y., Liu, Y. L., Zhang, Y. F., Cao, Y., Chen, Y. K., Li,
- 795 L., Liu, H. J., Cao, J. J., and Li J. J.: Influence of vertical transport on chemical evolution of dicarboxylic
- acids and related secondary organic aerosol from surface emission to the top of Mount Hua, Northwest China.
- 797 Sci. Total Environ., 858, 159892, http://dx.doi.org/10.1016/j.scitotenv.2022.159892, 2023.
- 798 Shen, M. X., Ho, K. F., Dai, W. T., Liu, S. X., Zhang, T., Wang, Q. Y., Meng, J. J., Chow, J. C., Watson, J.
- 799 G., Cao, J. J., and Li. J. J.: Distribution and stable carbon isotopic composition of dicarboxylic acids,
- 800 ketocarboxylic acids and α-dicarbonyls in fresh and aged biomass burning aerosols. Atmos. Chem. Phys.,
- 801 22(11), 7489–7504, <a href="https://doi.org/10.5194/acp-22-7489-2022">https://doi.org/10.5194/acp-22-7489-2022</a>, 2022.
- 802 Shen, M. X., Qi, W. N., Liu, Y. L., Zhang, Y. F., Dai, W. T., Li, L., Guo, X., Cao, Y., Jiang, Y. K., Wang, Q.,
- 803 Li, S. C., Wang, Q. Y., and Li, J. J: Measurement report: Observational insights into the impact of dust
- 804 transport on atmospheric dicarboxylic acids in ground region and free troposphere. Zenodo [data set],
- 805 <a href="https://zenodo.org/doi/10.5281/zenodo.15788834">https://zenodo.org/doi/10.5281/zenodo.15788834</a>, 2025.
- 806 Sullivan, R. C., and Prather, Kimberly A. Investigations of the diurnal cycle and mixing state of oxalic acid
- 807 in individual particles in Asian aerosol outflow. Environ. Sci. Technol. 41(23), 8062-8069,
- 808 https://doi.org/10.1021/es071134g, 2007a.
- 809 Sullivan, R. C., Guazzotti 1, S. A., Sodeman, D. A., and K. A. Prather.: Direct observations of the atmospheric
- processing of Asian mineral dust. Atmos. Chem. Phys., 7(5), 1213–1236, https://doi.org/10.5194/acp-7-
- 811 1213-2007, 2007b.
- 812 Sun, J. M., Zhang, M. Y., and Liu, T. S.: Spatial and temporal characteristics of dust storms in China and its
- surrounding regions, 1960–1999: Relations to source area and climate. J. Geophys. Res., 106(D10), 10,325–
- 814 10,333, https://doi.org/10.1029/2000JD900665, 2001.
- 815 Usher C. R., Michel, A. E. and Vicki H.: Grassian Reactions on Mineral Dust Chem. Rev. 103(12),
- 816 4883–4939. https://doi.org/10.1021/cr020657y, 2003.

- Vergara-Temprado, J., Miltenberger, A. K., Furtado, K., Grosvenor, D. P., Shipway, B. J., Hill, A. A.,
- Wilkinson, J. M., Field, P. R., Murray, B. J., and Carslaw, K. S.: Strong control of southern ocean cloud
- 819 reflectivity by ice-nucleating particles. Proc. Natl. Acad. Sci. U.S.A 115(11), 2687–2692.
- 820 https://doi.org/10.1073/pnas.1721627115, 2018.
- Wang, G. H., Kawamura, K., Cheng, C. L., Li, J. J., Cao, J. J., Zhang, R. J., Zhang, T., Liu, S. X., and Zhao,
- 822 Z. Z.: Molecular distribution and stable carbon isotopic composition of dicarboxylic acids, ketocarboxylic
- 823 acids, and α-dicarbonyls in size-resolved atmospheric particles from Xi'an city, China. Environ. Sci.
- 824 Technol., 46(9), 4783–4791. <a href="https://doi.org/10.1021/es204322c">https://doi.org/10.1021/es204322c</a>, 2012.
- Wang, G. H., Kawamura, K., Umemoto, N., Xie, M. J., Hu, S. Y., and Wang, Z. F.: Water-soluble organic
- 826 compounds in PM<sub>2.5</sub> and size-segregated aerosols over Mount Tai in North China Plain. J. Geophys. Res.
- 827 <u>114, 1–10. https://doi.org/10.1029/2008jd011390. D19208, 2009.</u>
- Wang, G. H., Cheng, C. L., Meng, J. J., Huang, Y., Li, J.J. and Ren, Y. Q.: Field observation on secondary
- 829 organic aerosols during Asian dust storm periods: Formation mechanism of oxalic acid and related
- 830 compounds on dust surface. Atmos. Environ., 113, 169–176. https://doi.org/10.1016/j.atmosenv.2015.05.013,
- 831 2015.
- 832 Wang, G. H., Zhang, S., Wu, C., Zhu, T., Xu, X. B., Ge, S. S., Sun, H. T., Sun Z. R., Wang, J. X., Ji, Y. M.,
- 833 Gao, J., Ren, Y. Q., Li, H., Zhang, F., Wang, Y., and Seinfeld, J. H.: Atmospheric sulfate aerosol formation
- enhanced by interfacial anions. PNAS Nexus, 4, pgaf058. https://doi.org/10.1093/pnasnexus/pgaf058, 2025.
- Wang, Y. D., Zhou, L., Wang, W. G., and Ge, M. F.: Heterogeneous uptake of formic acid and acetic acid on
- 836 mineral dust and coal fly ash. ACS Earth Space Chem. 4(2), 202-210,
- https://dx.doi.org/10.1021/acsearthspacechem.9b00263, 2020.
- 838 Wang, Z., Shi, C., Zhang, H., Chen, Y. J., Chi, X. Y., Xia, C., Wang, S. Y., Zhu, Y. Z., Zhang, K., Chen, X.
- 839 T., Xing, C., and Liu. C.: Measurement report: Dust and anthropogenic aerosols' vertical distributions over
- northern China dense aerosols gathered at the top of the mixing layer. Atmos. Chem. Phys., 23, 14271–14292,
- 841 <u>https://doi.org/10.5194/acp-23-14271-2023</u>, 2023.
- Warneck, P.: In-cloud chemistry opens pathway to the formation of oxalic acid in the marine atmosphere.
- 843 Atmos. Environ. 37(17), 2423–2427, https://doi.org/10.1016/S1352-2310(03)00136-5, 2003.
- Wu, C. L., Lin, Z. H., Shao, Y. P., Liu, X. H., and Li, Y.: Drivers of recent decline in dust activity over East

- 845 Asia, Nat. Commun., 13, 7105. https://doi.org/10.1038/s41467-022-34823-3, 2022.
- 846 Wu, F., Zhang, D. Z., Cao, J. J., Xu, H. M., and An, Z. S.: Soil-derived sulfate in atmospheric dust
- 847 particles at Taklimakan desert, Geophys. Res. Lett., 39(24), L24803,
- 848 <u>https://doi.org/10.1029/2012GL054406, 2012.</u>
- Xu, B. Q., Zhang, G., Gustafsson, Ö., Kawamura, K., Li, J., Andersson, A., Bikkina, S., Kunwar, B., Pokhrel,
- 850 A., Zhong, G. C., Zhao, S. Z., Li, J., Huang, C., Cheng, Z. N., Zhu, S. Y., Peng, P.A., and Sheng, G.Y.: Large
- contribution of fossil-derived components to aqueous secondary organic aerosols in China. Nat. Commun.
- 852 13, 5115. <a href="https://doi.org/10.1038/s41467-022-32863-3">https://doi.org/10.1038/s41467-022-32863-3</a>, 2022.
- 853 <u>Xu, W. Y., Kuang, Y., Liang, L. L., He, Y., Cheng, H. B., Bian, Y. X., Tao, J. C., Zhang, G., Zhao, P. S., Ma,</u>
- N., Zhao, H. R., Zhou, G. S., Su, H., Cheng, Y. F., Xu, X. B., Shao, M., amd Sun, Y. L.: Dust-dominated
- coarse particles as a medium for rapid secondary organic and inorganic aerosol formation in highly polluted
- 856 <u>air. Environ. Sci. Technol., 54(24):15710–15721. https://doi.org/10.1021/acs.est.0c07243, 2020.</u>
- Xu-Yang, Y. J. J., Skonieczny, C., Ayrault, S., Barbier, J., Bizeul, R., Bryskere, O., Chaboche, P., Chalaux-
- 858 Clergue, T., Corcho-Alvarado, J.A., Foucher, A., Karsenti, A., Leblanc, M., Orizaola, G., Plautre, A., Röllin,
- 859 S., Taraconat, N., Tenaud, N., Valdés, A. E., Dulac, F., and Evrard, O.: Radioactive contamination transported
- to Western Europe with Saharan dust. Sci. Adv., 11(5), eadr9192. https://doi.org/10.1126/sciadv.adr9192,
- 861 2025.
- Yang, C., Zhou, S. X., Zhang, C. Y., Yu, M. Y., Cao, F., and Zhang, Y. L.: Atmospheric chemistry of oxalate:
- Insight into the role of relative humidity and aerosol acidity from high-resolution observation. J. Geophys.
- 864 Res. Atmos., 127(4), e2021JD035364. https://doi.org/10.1029/2021JD035364, 2022.
- 865 Yang, J., Zhao, W. Y., Wei, L. F., Zhang, Q., Zhao, Y., Hu, W., Wu, L. B., Li, X. D., Pavuluri, C. M., Pan, X.
- 866 L., Sun, Y. L., Wang, Z. F., Liu, C. Q., Kawamura, K., and Fu, P. Q.: Molecular and spatial distributions of
- 867 dicarboxylic acids, oxocarboxylic acids, and-dicarbonyls in marine aerosols from the South China Sea to the
- 868 eastern Indian Ocean, Atmos. Chem. Phys., 20(11), 6841–6860, <a href="https://doi.org/10.5194/acp-20-6841-2020">https://doi.org/10.5194/acp-20-6841-2020</a>,
- 869 2020.
- Yamaguchi, N., Baba, T., Ichijo, T., Himezawa, Y., Enoki, K., Saraya, M., Li, P., and Nasu, M.: Abundance
- and community structure of bacteria on Asian dust particles collected in Beijing, China, during the Asian
- 872 Dust Season. Biol. Pharm. Bull., 39(1):68–77. https://doi.org/10.1248/bpb.b15-00573, 2016.

- Yang, Y., Russell, L. M., Lou, S. J., Liao, H., Guo, J. P., Liu, Y., Singh, B., and Ghan, S. J.: Dust-wind
- 874 interactions can intensify aerosol pollution over eastern China. Nat. Commun., 8:15333.
- 875 <u>https://doi.org/10.1038/ncomms15333</u>, 2017.
- Yermakov, A. N., Aloyan, A. E., Arutyunyan, V. O., and Pronchev, G. B.: On the mechanism of sulfur dioxide
- 877 oxidation in cloud drops. Izv. Atmos. Oceanic Phys., 59(5), 538-547.
- 878 https://doi.org/10.1134/S0001433823050055, 2023.
- 879 Yu, Z.C., and Jang M.: Atmospheric processes of aromatic hydrocarbons in the presence of mineral dust
- 880 particles in an urban environment. ACS Earth Space Chem., 3(11), 2404-2414.
- https://doi.org/10.1021/acsearthspacechem.9b00195, 2019.
- Yu, Z. C., Song, R. Y., Wang, Q. H., Quan, J. Y., Zhang, H. Y., Fu, J. J., and Jiang, G. B.: Research progress
- of atmospheric chemical process of airborne dust particles. Environ. Chem., 44(3): 854-867.
- 884 <u>https://doi.org/10.7524/j.issn.0254-6108.2024051303</u>, 2025.
- 885 Zhang, G. H., Lin, Q. H., Peng, L., Yang, Y. X., Jiang, F., Liu, F. X., Song, W., Chen, D. H., Cai, Z., Bi,
- 886 X. H., Miller, M., Tang, M. J., Huang, W. L., Wang, X. M., Peng, P. A., and Sheng, G. Y.: Oxalate
- 887 <u>formation enhanced by Fe-containing particles and environmental implications. Environ. Sci. Technol.</u>
- 888 <u>53(3):1269–1277. https://doi.org/10.1021/acs.est.8b05280, 2019.</u>
- Zhang, R. F., Gen, M. S., Liang, Z. C., Li, Y. J., and Chan, C. K.: Photochemical reactions of glyoxal
- 890 during particulate ammonium nitrate photolysis: brown carbon formation, enhanced glyoxal decay, and
- 891 organic phase formation. Environ. Sci. Technol., 56(3), 1605–1614.
- 892 <u>https://doi.org/10.1021/acs.est.1c07211, 2022.</u>
- Zhang, S., Xu, H., Lan, J. H., Goldsmith, Y., Torfstein, A., Zhang, G. L., Zhang, J., Song, Y. P., Zhou, K.,
- Tan, L.C., Xu, S., Xu, X. M., and Enzel, Y.: Dust storms in northern China during the last 500 years. Sci.
- 895 China Earth Sci., 64(5), 813–824. https://doi.org/10.1007/s11430-020-9730-2, 2021.
- Zhu, Q. Z., and Liu, Y. J.: The dominant factor in extreme dust events over the Gobi Desert is shifting from
- extreme winds to extreme droughts. Npj clim. Atmos. Sci., 7:141, https://doi.org/10.1038/s41612-024-
- 898 <u>00689-z</u>, 2024.
- 899 Zhang, T., Cao, J. J., Tie, X. X., Shen, Z. X., Liu, S. X., Ding, H., Han, Y. M., Wang, G. H., Ho, K. F., Qiang,
- J., and Li, W. T.: Water-soluble ions in atmospheric aerosols measured in Xi'an, China: Seasonal variations

- 901 and sources. Atmos. Res., 102(1–2), 110–119. <a href="https://doi.org/10.1016/j.atmosres.2011.06.014">https://doi.org/10.1016/j.atmosres.2011.06.014</a>, 2011.
- 902 Zhao, W.Y., and Fu, P.Q.: Characterization of dicarboxylic acids, oxocarboxylic acids, and α-dicarbonyls in
- 903 atmospheric aerosols: A review. Chinese Journal of Ecology, 37, 265-277. https://doi.10.13292/j.1000-
- 904 <u>4890.201801.002</u>, 2018.

- 905 Zheng, F. X., Li, J. W., Hua, C. J., Xie, J. L., Zhang, Y. S., Li, L.Y., Shen, S. N., Hakala, S., Yan, C., Feng,
- 2. M., Fan, X. L., Bianchi, F., Petäjä, T., Kerminen, V., Kulmala, M., Xia, M., Zha, Q., Du, W., Daellenbach,
- 907 K. R., Cai, J., and Liu, Y. C.: Dust event identification and characterization with one-year online observations
- 908 in Beijing. Sci. Total Environ., 956(15), 177296. https://doi.org/10.1016/j.scitotenv.2024.177296, 2024.
- 209 Zhi, M. K., Wang, G. C., Xu, L., Li, K. I., Nie, W., Niu, H. Y., Shao, L. Y., Liu, Z. R., Yi, Z.W., Wang,
- 910 Y. T., Shi, Z. B., Ito, A., Zhai, S. X., and Li, W. J.: How acid iron dissolution in aged dust particles
- 911 responds to the buffering capacity of carbonate minerals during Asian dust storms. Environ. Sci.
- 912 <u>Technol.</u>, 59(12): 6167–6178. https://doi.org/10.1021/acs.est.4c12370, 2025.

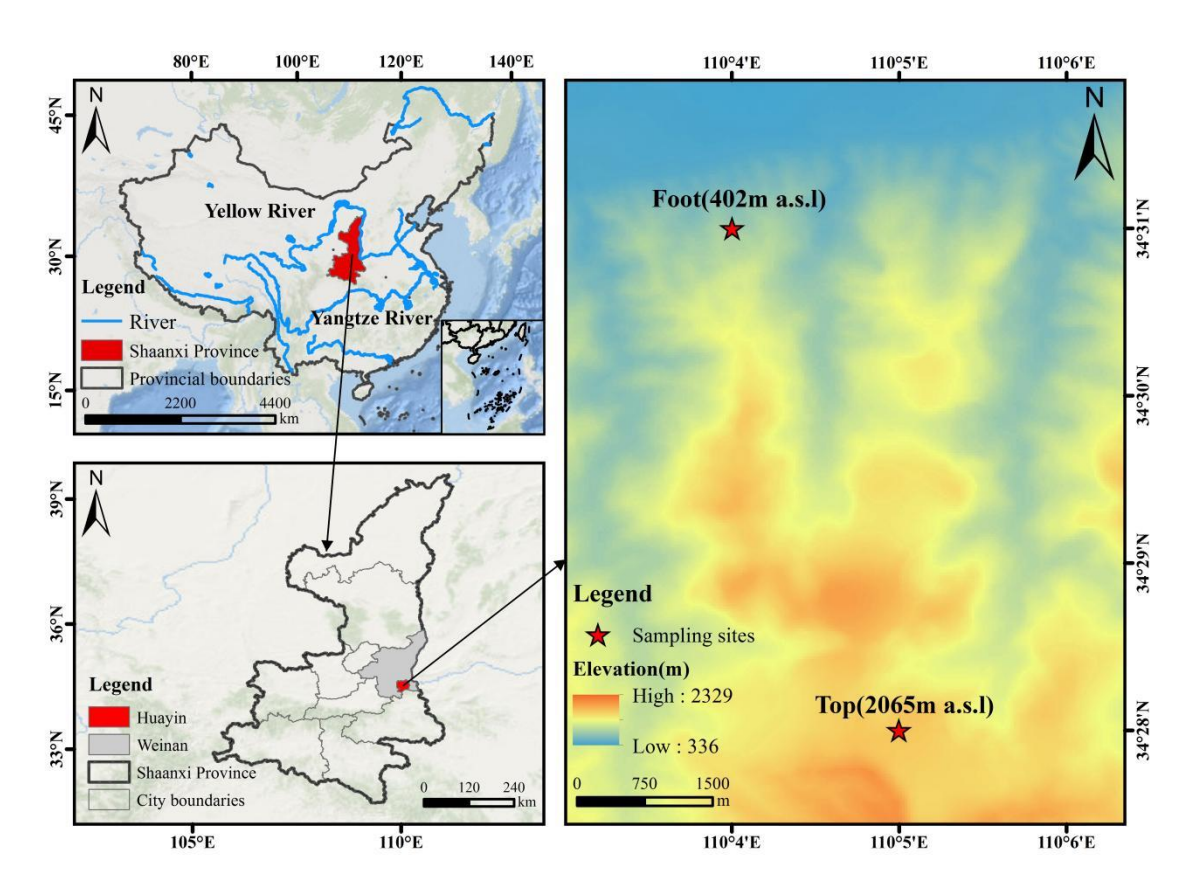


Figure 1 Distribution of aerosol sampling sites at the foot and top of Mount Hua (December 2020 to January 2021)

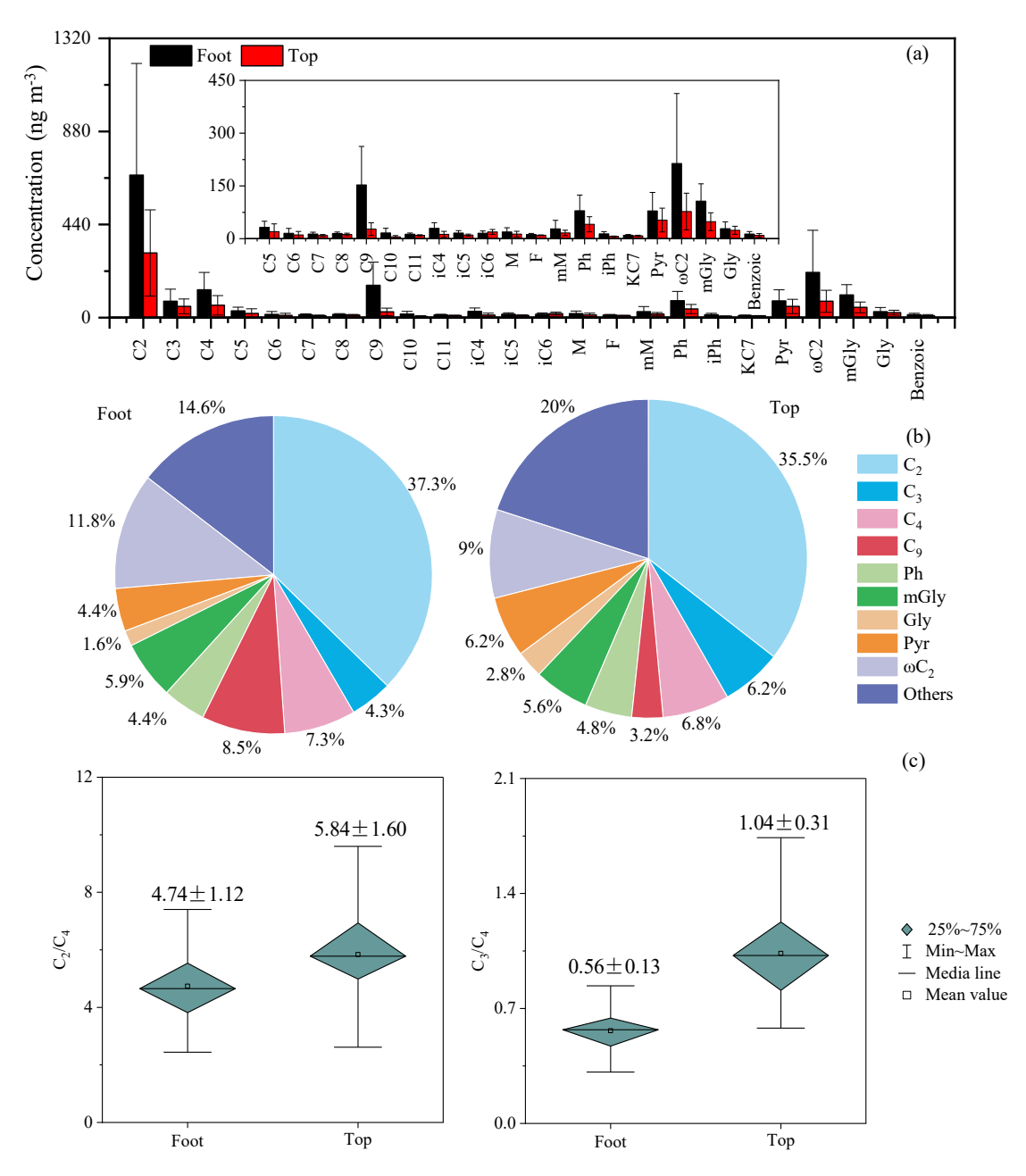


Figure 2 Molecular distribution of dicarboxylic acids and related Compounds (a), relative percentages of major dicarboxylic acids (b), and ratios of  $C_2/C_4$  and  $C_3/C_4$  (c) at the foot and top of Mount Hua during non-dust periods

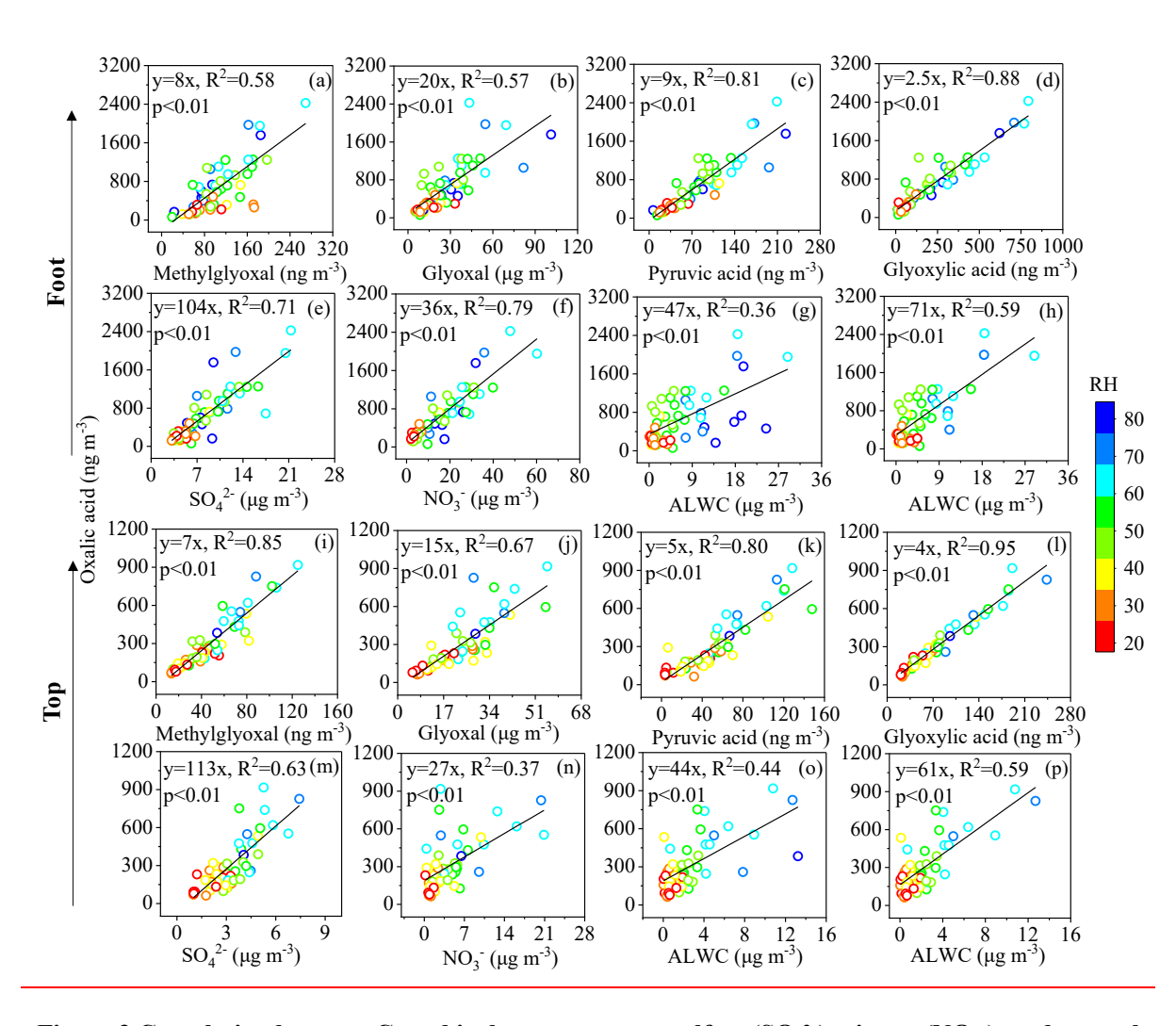


Figure 3 Correlation between  $C_2$  and its key precursors, sulfate ( $SO_4^{2-}$ ), nitrate ( $NO_3^-$ ), and aerosol liquid water content (ALWC) at the foot and top of Mount Hua with varying relative humidity (RH)

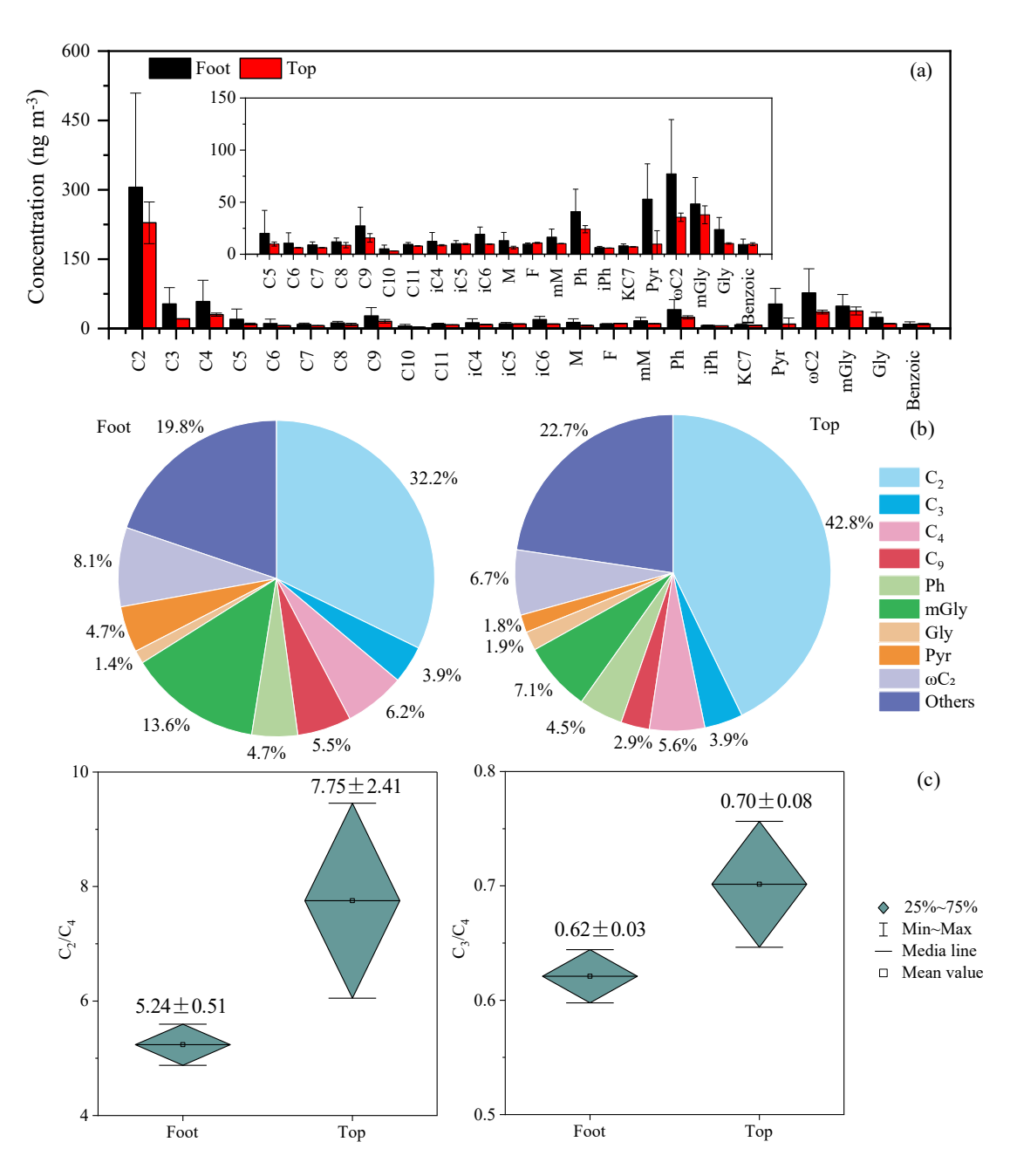


Figure 4 Molecular distribution of dicarboxylic acids and related compounds (a), relative percentages of major dicarboxylic acids (b), and ratios of  $C_2/C_4$  and  $C_3/C_4$  (c) at the foot and top of Mount Hua during dust events

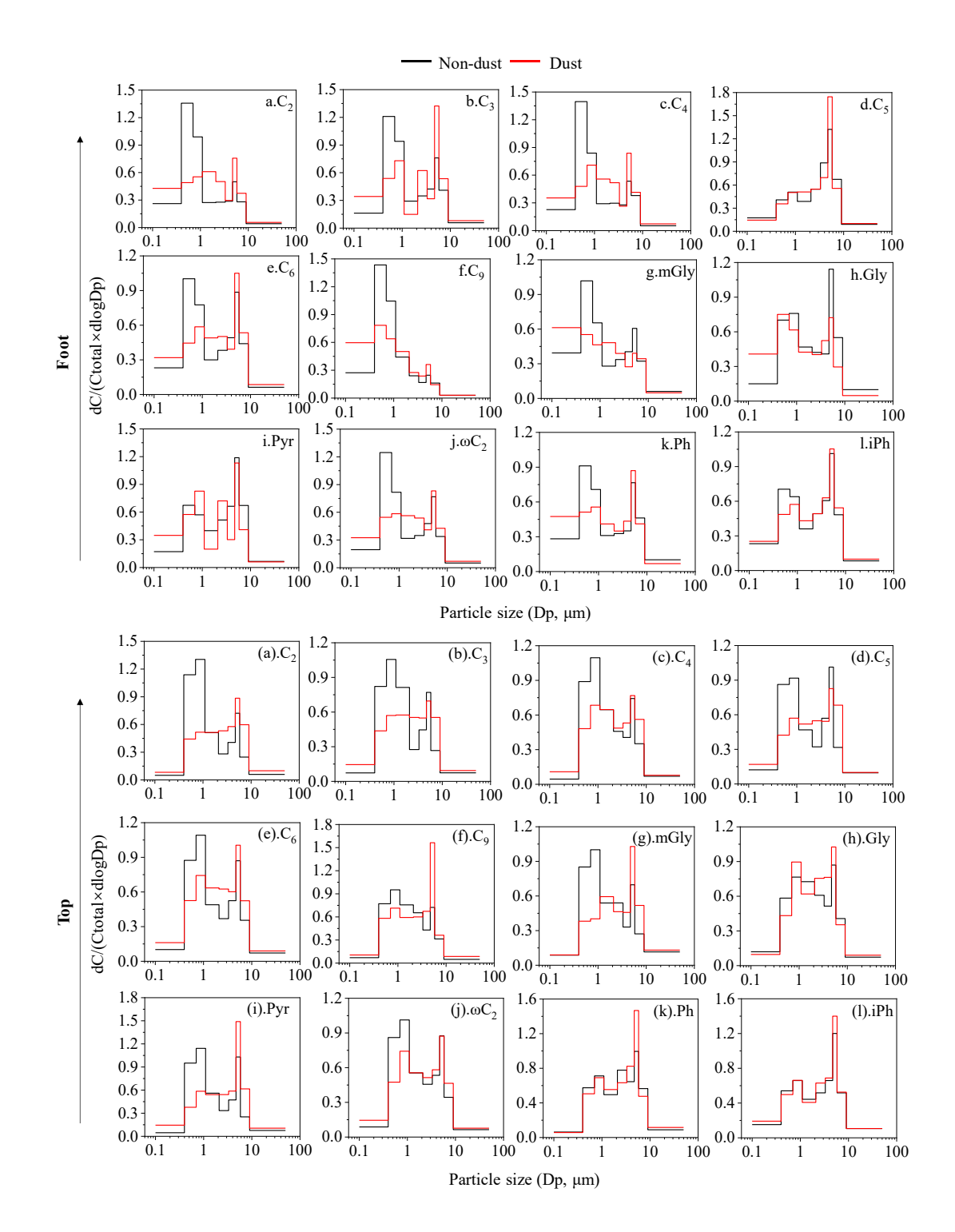


Figure 5 Size Distribution distribution patterns of dicarboxylic acids at the foot and top of Mount

Hua during non-dust and dust periods

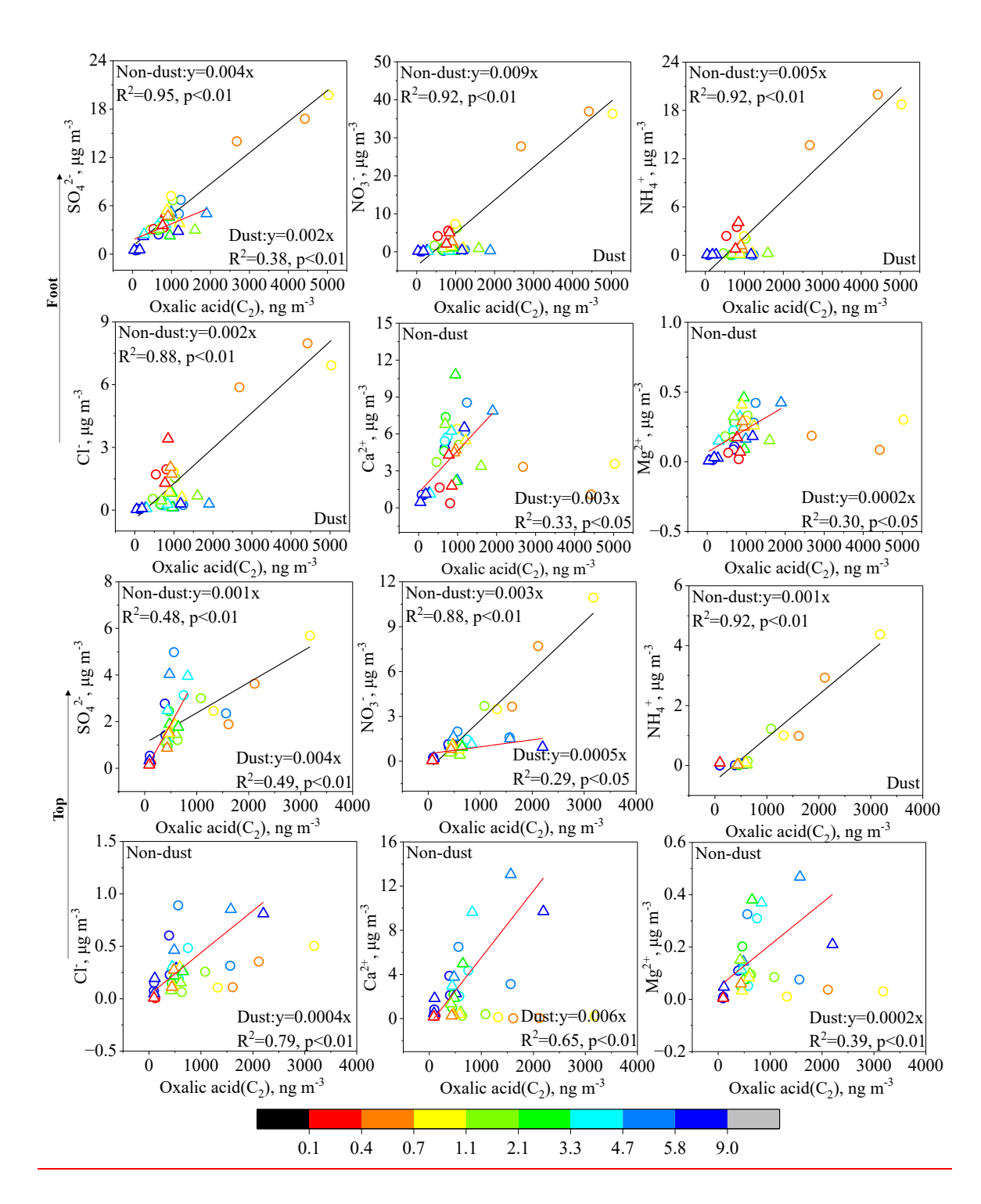


Figure 6 Correlation of C<sub>2</sub> with water-soluble ions at the foot and top of Mount Hua during non-dust and dust periods (Circles in the figure represent non-dust periods, and triangles represent dust periods)

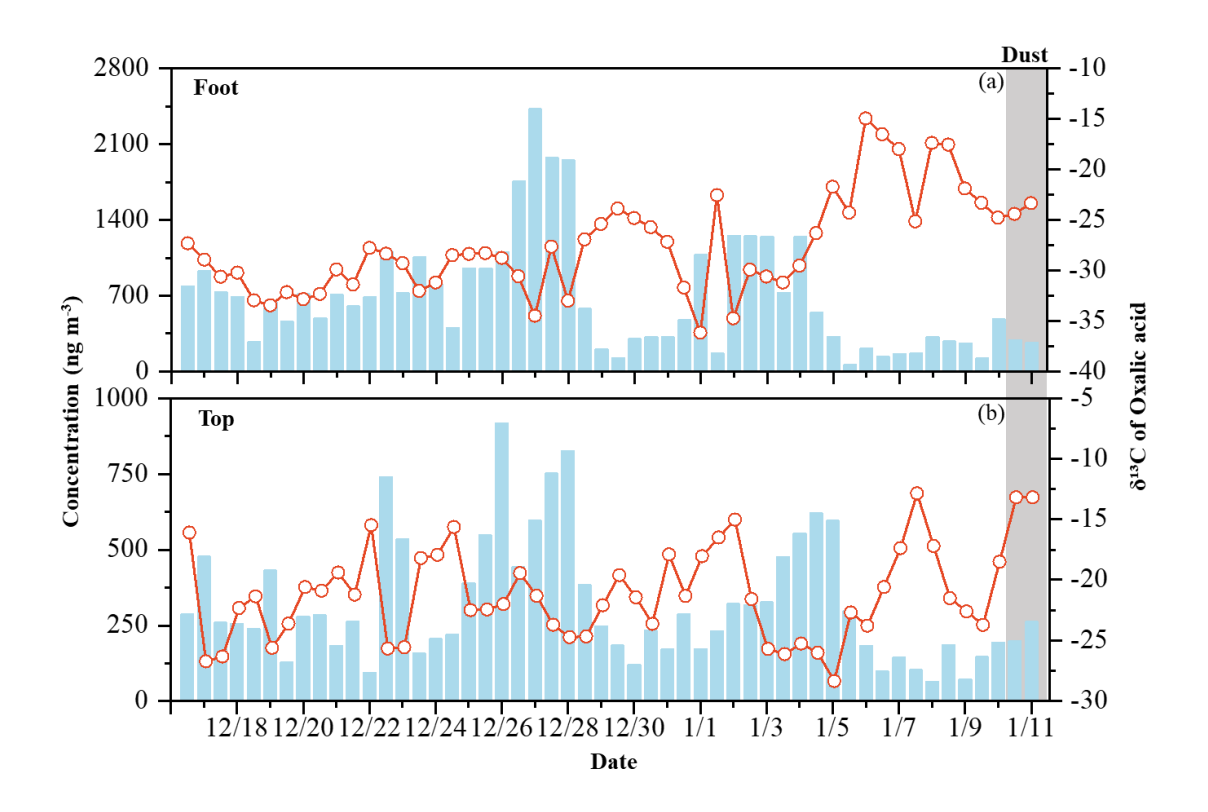


Figure 7 Stable carbon isotopes (δ¹³C) of C₂ in PM₂.5 at the foot and top of Mount Hua

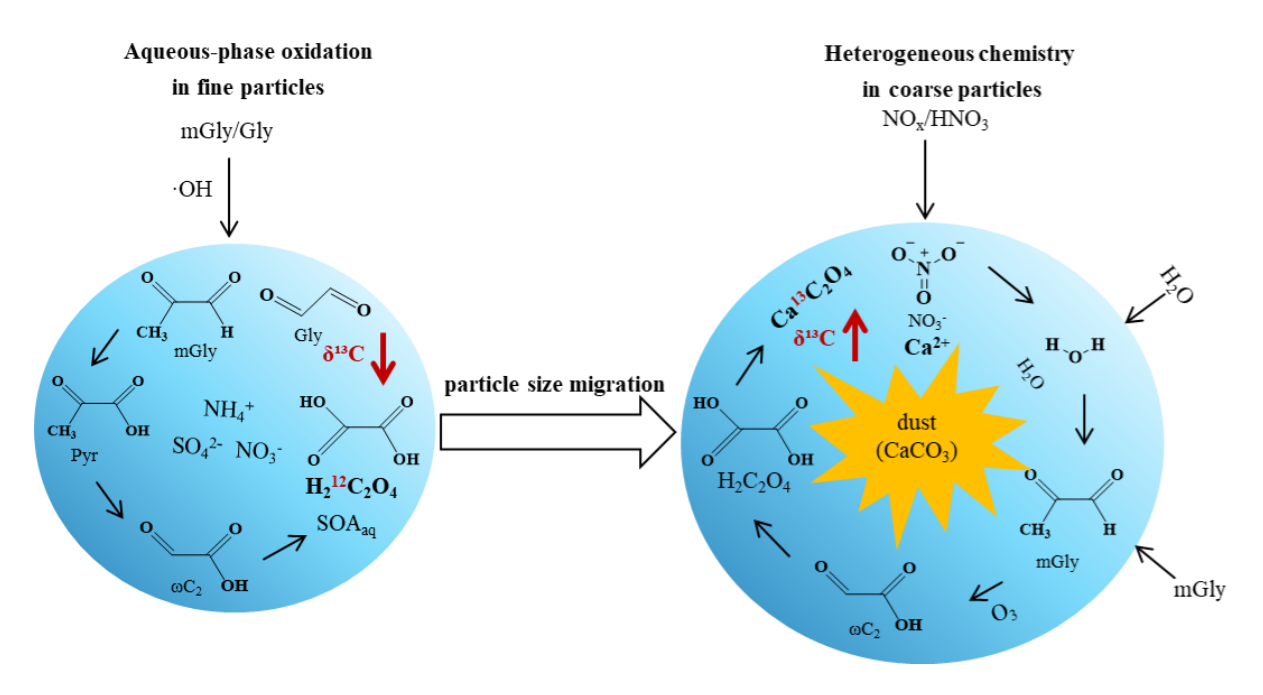


Figure 8 Mechanism diagram of dust-driven particle-size migration and formation pathways of  $C_2\,$ 

|                                      |                | Foot          | Тор             |               |               |               |           |  |  |  |
|--------------------------------------|----------------|---------------|-----------------|---------------|---------------|---------------|-----------|--|--|--|
| Compound                             | Daytime        | Nighttime     | Whole           | Daytime       | Nighttime     | Whole         | $R_{F/T}$ |  |  |  |
|                                      | (N = 26)       | (N = 27)      | (N = 53)        | (N = 26)      | (N = 27)      | (N = 53)      |           |  |  |  |
| Dicarboxylic acids                   |                |               |                 |               |               |               |           |  |  |  |
| Oxalic, C <sub>2</sub>               | $766 \pm 552$  | $585 \pm 497$ | $674 \pm 528$   | $312 \pm 224$ | $299 \pm 186$ | $306 \pm 204$ | 2.2       |  |  |  |
| Malonic, C <sub>3</sub>              | $86 \pm 58$    | $71 \pm 55$   | $78 \pm 56$     | $54\pm39$     | $53\pm32$     | $53\pm35$     | 1.5       |  |  |  |
| Succinic, C <sub>4</sub>             | $152\pm83$     | $112\pm77$    | $132\pm82$      | $60 \pm 47$   | $57 \pm 46$   | $58 \pm 46$   | 2.3       |  |  |  |
| Glutaric, C <sub>5</sub>             | $38\pm19$      | $27\pm14$     | $32\pm17$       | $22 \pm 27$   | $18 \pm 16$   | $20\pm22$     | 1.6       |  |  |  |
| Adipic, C <sub>6</sub>               | $17 \pm 15$    | $14\pm13$     | $15\pm14$       | $12\pm13$     | $10\pm6.3$    | $11 \pm 9.8$  | 1.4       |  |  |  |
| Pimelic, C <sub>7</sub>              | $15 \pm 5.0$   | $12\pm5.0$    | $13 \pm 5.1$    | $9.2 \pm 3.3$ | $8.9 \pm 2.3$ | $9.0 \pm 2.8$ | 1.4       |  |  |  |
| Suberic, C <sub>8</sub>              | $16 \pm 4.1$   | $14\pm3.4$    | $15\pm3.8$      | $13\pm3.7$    | $12\pm3.5$    | $12\pm3.6$    | 1.3       |  |  |  |
| Azelaic, C9                          | $175\pm110$    | $131\pm106$   | $153\pm110$     | $28\pm19$     | $27\pm17$     | $27\pm18$     | 5.7       |  |  |  |
| Sebacic, C <sub>10</sub>             | $19\pm15$      | $14\pm11$     | $16\pm14$       | $5.3\pm3.5$   | $5.3 \pm 3.7$ | $5.3 \pm 3.5$ | 3.0       |  |  |  |
| Undecanedioic, C <sub>11</sub>       | $14 \pm 3.8$   | $12\pm2.5$    | $13\pm3.3$      | $9.9 \pm 1.8$ | $9.2\pm1.7$   | $9.6 \pm 1.8$ | 1.4       |  |  |  |
| Methylmalonic, iC <sub>4</sub>       | $36\pm17$      | $24\pm13$     | $29\pm16$       | $13 \pm 9.4$  | $12\pm7.6$    | $13\pm8.5$    | 2.2       |  |  |  |
| Mehtylsuccinic, iC5                  | $16 \pm 5.4$   | $16 \pm 7.9$  | $16 \pm 6.7$    | $10\pm3.2$    | $10\pm2.4$    | $10\pm2.8$    | 1.6       |  |  |  |
| Methylglutaric, iC <sub>6</sub>      | $18 \pm 6.7$   | $14 \pm 5.4$  | $16 \pm 6.3$    | $19\pm7.7$    | $19 \pm 6.2$  | $19 \pm 6.9$  | 0.8       |  |  |  |
| Maleic, M                            | $22 \pm 12$    | $17 \pm 11$   | $19 \pm 12$     | $13 \pm 10$   | $13 \pm 5.7$  | $13\pm7.9$    | 1.5       |  |  |  |
| Fumaric, F                           | $13 \pm 3.4$   | $11\pm2.4$    | $12\pm3.0$      | $10\pm1.2$    | $10\pm1.0$    | $9.7 \pm 1.1$ | 1.2       |  |  |  |
| Methylmaleic, mM                     | $29\pm18$      | $27\pm29$     | $28\pm24$       | $17 \pm 9.1$  | $16\pm6.2$    | $16\pm7.7$    | 1.8       |  |  |  |
| Phthalic, Ph                         | $89 \pm 43$    | $71 \pm 45$   | $80 \pm 44$     | $44\pm23$     | $39\pm20$     | $41\pm22$     | 2.0       |  |  |  |
| Isophthalic, iPh                     | $15 \pm 5.4$   | $13\pm7.0$    | $14 \pm 6.3$    | $6.5\pm1.2$   | $6.5 \pm 0.8$ | $6.5\pm1.0$   | 2.2       |  |  |  |
| Ketopimelic, kC7                     | $10.2\pm2.3$   | $9.4 \pm 2.1$ | $9.8 \pm 2.2$   | $8.3\pm1.9$   | $8.0 \pm 1.7$ | $8.1\pm1.8$   | 1.2       |  |  |  |
|                                      |                | Kete          | ocarboxylic ac  | eids          |               |               |           |  |  |  |
| Pyruvic, Pyr                         | 85 ± 45        | 73 ± 59       | 79 ± 53         | 52 ± 38       | 54 ± 30       | 53 ± 34       | 1.5       |  |  |  |
| Glyoxylic, ωC <sub>2</sub>           | $230 \pm 201$  | $198\pm200$   | $214\pm199$     | $79 \pm 58$   | $75 \pm 47$   | $77 \pm 52$   | 2.8       |  |  |  |
| α-Dicarbonyls                        |                |               |                 |               |               |               |           |  |  |  |
| Glyoxal, Gly                         | 29 ± 15        | 29 ± 23       | 29 ± 19         | 23 ± 13       | 24 ± 10       | 24 ± 12       | 1.2       |  |  |  |
| Methylglyoxal,<br>mGly               | $128\pm49$     | 87 ± 42       | $107 \pm 49$    | $49\pm28$     | $48\pm23$     | $48\pm25$     | 2.2       |  |  |  |
| Others                               |                |               |                 |               |               |               |           |  |  |  |
| Benzoic, Ha                          | 15 ± 7.1       | $12 \pm 6.7$  | 13 ± 6.9        | $9.6 \pm 5.4$ | 9.3 ± 5.1     | $9.4 \pm 5.2$ | 1.4       |  |  |  |
| Total detected (ng m <sup>-3</sup> ) | 2029 ±<br>1294 | 1594 ± 1238   | $1807 \pm 1280$ | $879 \pm 591$ | $842 \pm 481$ | $860 \pm 534$ | 2.1       |  |  |  |

|                                      |         | Foot      |               | Тор     |           |  |  |  |  |
|--------------------------------------|---------|-----------|---------------|---------|-----------|--|--|--|--|
| Compound                             | Daytime | Nighttime | Whole         | Daytime | Nighttime | Whole  |  |  |  |
|                                      | (N=1)   | (N=1)     | (N=2)         | (N=1)   | (N=1)     | (N=2)  |  |  |  |
| Oxalic, C <sub>2</sub>               | 289     | 262       | $276 \pm 20$  | 261     | 197       | $229 \pm 45$                                 |  |  |  |
| Malonic, C <sub>3</sub>              | 28      | 38        | $33 \pm 7.3$  | 21      | 21        | $21 \pm 0.1$<br>$30 \pm 3.5$<br>$10 \pm 1.9$ |  |  |  |
| Succinic, C <sub>4</sub>             | 47      | 59        | $53 \pm 8.9$  | 28      | 33        |  |  |  |  |
| Glutaric, C <sub>5</sub>             | 15      | 16        | $15\pm0.5$    | 8.4     | 11        |  |  |  |  |
| Adipic, C <sub>6</sub>               | 9.8     | 10.2      | $10 \pm 0.3$  | 6.2     | 6.4       | $6.3\pm0.2$                                  |  |  |  |
| Pimelic, C <sub>7</sub>              | 7.6     | 9.2       | $8.4 \pm 1.1$ | 6.3     | 6.3       | $6.3 \pm 0.0$                                |  |  |  |
| Suberic, C <sub>8</sub>              | 9.2     | 11        | $10\pm1.3$    | 6.9     | 11        | $8.7 \pm 2.6$                                |  |  |  |
| Azelaic, C9                          | 41      | 54        | $47 \pm 9.4$  | 13      | 19        | $16 \pm 4.1$                                 |  |  |  |
| Sebacic, C <sub>10</sub>             | 4.7     | 5.6       | $5.1 \pm 0.7$ | 3.2     | 3.2       | $3.2 \pm 0.0$                                |  |  |  |
| Undecanedioic, C <sub>11</sub>       | 9.3     | 10        | $9.8 \pm 0.7$ | 8.0     | 7.9       | $8.0 \pm 0.0$                                |  |  |  |
| Methylmalonic, iC <sub>4</sub>       | 15      | 16        | $16 \pm 0.3$  | 8.2     | 9.1       | $8.7 \pm 0.6$                                |  |  |  |
| Mehtylsuccinic, iC <sub>5</sub>      | 12      | 11        | $12 \pm 0.9$  | 9.4     | 10.2      | $9.8 \pm 0.6$                                |  |  |  |
| Methylglutaric, iC <sub>6</sub>      | 15      | 16        | $16 \pm 0.3$  | 9.5     | 10.0      | $9.8 \pm 0.3$                                |  |  |  |
| Maleic, M                            | 7.8     | 10        | $9.1\pm1.8$   | 7.3     | 5.6       | $6.4\pm1.3$                                  |  |  |  |
| Fumaric, F                           | 13      | 15        | $14\pm1.4$    | 10.5    | 11.3      | $10.9 \pm 0.6$                               |  |  |  |
| Methylmaleic, mM                     | 12      | 13        | $13\pm0.2$    | 10.3    | 10.2      | $10.3\pm0.0$                                 |  |  |  |
| Phthalic, Ph                         | 39      | 41        | $40\pm1.3$    | 22      | 27        | $24\pm3.5$                                   |  |  |  |
| Isophthalic, iPh                     | 9.5     | 12        | $11 \pm 1.6$  | 5.9     | 5.9       | $5.9 \pm 0.0$                                |  |  |  |
| Ketopimelic, kC7                     | 7.5     | 7.9       | $7.7 \pm 0.3$ | 7.2     | 7.1       | $7.2 \pm 0.1$                                |  |  |  |
| Pyruvic, Pyr                         | 29      | 52        | $40\pm17$     | 0.6     | 19        | $9.8 \pm 13$                                 |  |  |  |
| Glyoxylic, ωC <sub>2</sub>           | 51      | 87        | $69\pm26$     | 33      | 38        | $36 \pm 4.0$                                 |  |  |  |
| Glyoxal, Gly                         | 14      | 8.7       | $12 \pm 4.1$  | 9.8     | 10.9      | 10.4± 0.7                                    |  |  |  |
| Methylglyoxal,<br>mGly               | 92      | 140       | $116 \pm 34$  | 32      | 44        | $38 \pm 8.6$                                 |  |  |  |
| Benzoic, Ha                          | 12      | 17        | $15 \pm 3.8$  | 8.7     | 10.7      | $9.7 \pm 1.4$                                |  |  |  |
| Total detected (ng m <sup>-3</sup> ) | 761     | 949       | 855 ± 142     | 535     | 533       | $534 \pm 92$                                 |  |  |  |

Table 3 Comparison of concentrations of dicarboxylic acids and related compounds in particulate matter of different particle size ranges ( $\leq$ 2.1  $\mu$ m and >2.1  $\mu$ m) at the foot and top of Mount Hua during non-dust and dust periods

|   | Foot       |            |            |            |            |            | Тор        |            |            |            |                  |            |  |
|---|------------|------------|------------|------------|------------|------------|------------|------------|------------|------------|------------------|------------|--|
| C1  | Non        | -dust Dust |            | ıst        | $R_{D/N}$  |            | Non-dust   |            | Dust       |            | R <sub>D/N</sub> |            |  |
| Compound                                  | ≤2.1<br>μm | >2.1<br>μm | ≤2.1<br>μm | >2.1<br>μm | ≤2.1<br>µm | >2.1<br>µm | ≤2.1<br>µm | >2.1<br>μm | ≤2.1<br>µm | >2.1<br>µm | ≤2.1<br>μm       | >2.1<br>μm |  |
| Oxalic, C2                                | 8662       | 2718       | 4880       | 2843       | 0.3        | 0.6        | 5512       | 2217       | 2161       | 2301       | 0.4              | 1.1        |  |
| Malonic, C <sub>3</sub>                   | 750        | 388        | 361        | 371        | 0.5        | 1.0        | 757        | 359        | 305        | 253        | 0.5              | 0.8        |  |
| Succinic, C <sub>4</sub>                  | 1505       | 594        | 829        | 505        | 0.4        | 0.6        | 986        | 488        | 371        | 294        | 0.5              | 0.8        |  |
| Glutaric, C <sub>5</sub>                  | 238        | 350        | 199        | 297        | 1.5        | 1.5        | 557        | 390        | 334        | 324        | 0.7              | 1.0        |  |
| Adipic, C <sub>6</sub>                    | 427        | 277        | 347        | 292        | 0.6        | 0.8        | 457        | 275        | 290        | 240        | 0.6              | 0.8        |  |
| Azelaic, C9                               | 2313       | 371        | 1097       | 304        | 0.2        | 0.3        | 646        | 302        | 379        | 396        | 0.5              | 1.0        |  |
| Methylglyoxal,<br>mGly                    | 237        | 119        | 217        | 90         | 0.5        | 0.4        | 146        | 67         | 49         | 55         | 0.5              | 1.1        |  |
| <u>Glyoxal,</u> Gly                       | 312        | 268        | 237        | 145        | 0.9        | 0.6        | 192        | 129        | 140        | 114        | 0.7              | 0.8        |  |
| Pyruvic, Pyr                              | 729        | 800        | 687        | 513        | 1.1        | 0.7        | 1022       | 521        | 451        | 633        | 0.5              | 1.4        |  |
| Glyoxylic, ωC <sub>2</sub>                | 2181       | 1171       | 979        | 663        | 0.5        | 0.7        | 1138       | 678        | 658        | 545        | 0.6              | 0.8        |  |
| Phthalic, Ph                              | 1018       | 652        | 499        | 386        | 0.6        | 0.8        | 564        | 481        | 302        | 356        | 0.9              | 1.2        |  |
| Isophthalic, iPh<br>(ng m <sup>-3</sup> ) | 206        | 184        | 157        | 163        | 0.9        | 1.0        | 162        | 173        | 146        | 169        | 1.1              | 1.2        |  |